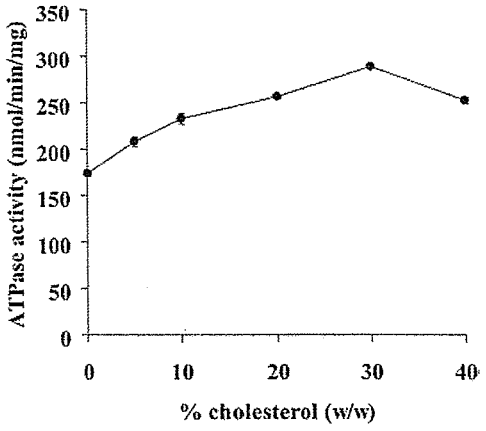

Figure 3 Effects of cholesterol on the basal ATPase activity

Purified MDR1 was reconstituted in PC/PE/PS (4:4:2) liposomes containing 0, 5, 10, 20, 30 or 40 % (w/w) cholesterol. Data are presented as means ± S.D. ($n = 3$).

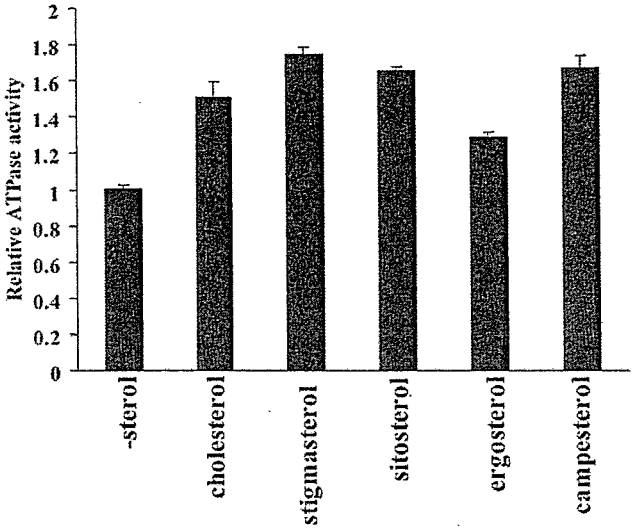

Figure 4 Effects of sterols on the basal ATPase activity

Purified MDR1 was reconstituted in liposomes containing 20 % (w/w) cholesterol, stigmasterol, β-sitosterol, ergosterol or campesterol. Relative ATPase activity is presented with respect to that in the absence of sterol (-sterol) ± S.D. ($n = 3$).

but showed strong inhibitory effects at higher concentrations and suppressed ATPase activity below the basal level (approx. 200 nmol/min/mg) at 200 μM or more. With increasing concentration of colchicine there was an increase in ATPase, but maximal activity was not obtained even at 2 mM. Without the reconstitution in liposomes, ATPase activity was not stimulated by the addition of substrate drugs (results not shown), suggesting that the lipid environment is quite important for the function of MDR1 as reported previously [22].

Effects of cholesterol on MDR1 ATPase activity

It has been suggested that the basal ATPase activity of human MDR1 in native membrane vesicles is highly dependent on the presence of cholesterol [23,24], and also that the basal ATPase activity of partially purified hamster MDR1, reconstituted in PC/PE (9:1) liposomes, is dependent on the presence of cholesterol [22]. We examined whether cholesterol affects the ATPase activity of purified human MDR1 by reconstituting the protein in liposomes (PC/PE/PS = 4:4:2) containing various concentrations of cholesterol (Figure 3). The ATPase activity increased as the concentration of cholesterol increased and peaked at 30 % (w/w) cholesterol. In the presence of 30 % cholesterol, the ATPase activity of MDR1 was 1.7-fold greater than ATPase activity in the absence of cholesterol. This suggests that cholesterol directly interacted with MDR1 at drug-binding sites. Alternatively, cholesterol may have affected the lipid environment, fluidity for example, and indirectly increased the turnover of basal ATP hydrolysis.

Effects of various sterols on basal activity

To consider the possibility of an indirect effect of cholesterol on MDR1, the specificity of sterol species was examined (Figure 4). Stigmasterol, sitosterol and campesterol stimulated the MDR1 ATPase activity as efficiently as cholesterol. Ergosterol was less effective than other sterols. The specific effect of sterols on MDR1 ATPase activity may support the direct interaction of sterols with MDR1.

Binding of [^{3}H]cholesterol to detergent soluble MDR1

The direct binding of cholesterol to purified MDR1 was confirmed by two methods, a pull-down assay and size-exclusion chromatography. We found that a significant amount of cholesterol bound to micelles of DDM and eluted in earlier fractions (fractions 3–5) in both the absence and presence of MDR1. Thus, for the *in vitro* cholesterol binding assay, the detergent was replaced with 0.1 % deoxycholate, which has a much higher c.m.c (critical micellar concentration) value and forms smaller micelles compared with those of DDM. MDR1 purified in 0.1 % deoxycholate showed as much ATPase activity as that purified in DDM when reconstituted in proteoliposomes. Moreover, when MDR1 purified in 0.1 % deoxycholate was reconstituted in liposomes containing 20 % cholesterol, the K_m value for verapamil was decreased from 4.7 ± 0.4 μM to 1.9 ± 0.2 μM as discussed later (Table 1). These results suggest that MDR1 purified in deoxycholate is catalytically active and has similar features to MDR1 purified in DDM.

The Ni-NTA pull-down assay revealed that [^{3}H]cholesterol was co-precipitated with MDR1, but not with KcsA, whereas similar amounts of MDR1 and KcsA were precipitated (Figure 5A). To investigate further the binding of cholesterol to purified MDR1, size-exclusion chromatography was used. Soluble MDR1 was mixed with the cholesterol–MβCD complex and loaded on to the column. When the cholesterol–MβCD complex was mixed with MDR1, cholesterol was co-eluted with MDR1 (Figure 5B). In contrast, most cholesterol was retained in the column and was not eluted from Sephadex G100 resin when the cholesterol–MβCD complex was applied to the column without MDR1, probably due to non-specific binding to the resin. The amount of cholesterol bound to MDR1 was correlated with the [^{3}H]cholesterol concentration and the amount of MDR1 (results not shown). Furthermore, the binding of [^{3}H]cholesterol to MDR1 was competitively inhibited by the unlabelled cholesterol–MβCD complex (Figure 5C).

Effect of cholesterol on the drug-stimulated ATPase activity of MDR1

MDR1 has been suggested to possess multiple drug-binding sites, and a drug binding to one site allosterically modulates drugs binding to other sites [13–15]. Because the above results suggested that cholesterol interacts directly with MDR1, we

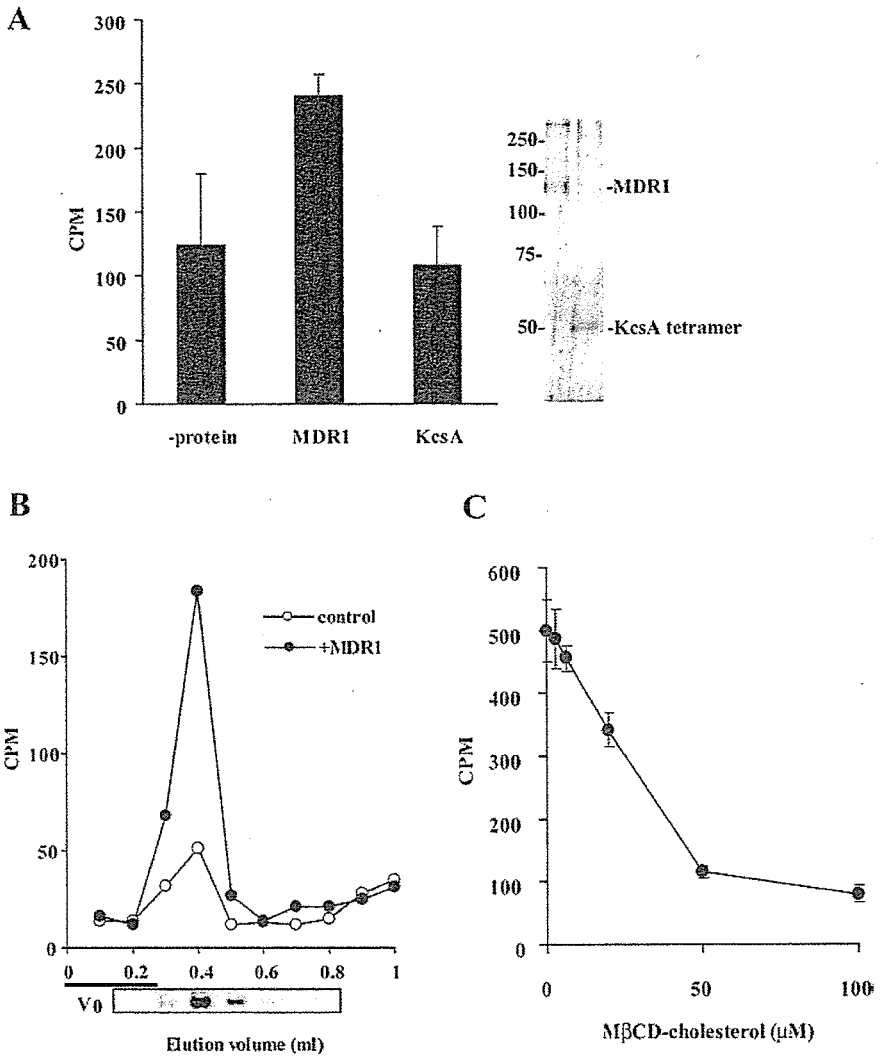

Figure 5 Binding of cholesterol to purified MDR1

(**A**) Purified proteins (6 μg) were mixed with 3 μM of the [^{3}H]cholesterol–MβCD complex at 37 °C for 2 min and Ni-NTA agarose was added. Proteins were eluted by 500 mM imidazole and analysed for radioactivity with a liquid-scintillation counter. Eluted protein was subjected to SDS/PAGE and visualized by silver-staining (right-hand panel). (**B**) Purified MDR1 (6 μg) was mixed with 3 μM [^{3}H]cholesterol–MβCD complex at 37 °C for 2 min then loaded on a column of Sephadex G100 (1 ml) and each fraction (10 × 100 μl) was analysed for radioactivity with a liquid-scintillation counter. MDR1 protein was visualized by silver staining after SDS/PAGE. The column void volume is shown as V_0. (**C**) Competitive inhibition of [^{3}H]cholesterol with unlabelled cholesterol. Purified MDR1 was mixed with 3 μM [^{3}H]cholesterol–MβCD complex and unlabelled cholesterol–MβCD complex. Fractions 3–6 were mixed and the amount of eluted [^{3}H]cholesterol was analysed.

expected cholesterol to affect the drug-stimulated ATPase activity of MDR1. We examined the drug-stimulated ATPase activity of MDR1 reconstituted either in liposomes (PC/PE/PS = 4:4:2) or in liposomes containing 20 % (w/w) cholesterol. In the cases of rhodamine 123 and digoxin, the presence of cholesterol had little affect on the V_{max} of ATPase activity but significantly lowered the K_m value from 21 to 10 μM (Figure 6A, Table 1) and from 181 to 76 μM (Figure 6B, Table 1) respectively.

In contrast, the presence of cholesterol had little affect on the K_m for paclitaxel, but increased the V_{max} from 160 to 411 nmol/min/mg (Figure 6C, Table 1). These results suggested that cholesterol affected the drug-stimulated ATPase activity of MDR1 and effects of cholesterol differed from one drug to another: the presence of cholesterol increases the affinity of MDR1 for rhodamine 123 and digoxin, whereas it increases the paclitaxel-induced hydrolysis of ATP by MDR1. K_m values for ATP were not affected by cholesterol in the absence or presence of paclitaxel (results not shown).

To further analyse effects of cholesterol on the drug-stimulated hydrolysis of ATP by MDR1, MDR1 was reconstituted in liposomes containing 0, 5, 10 or 20 % (w/w) cholesterol and the enzymatic parameters of ATPase activity for ten drugs, rhodamine 123, verapamil, dexamethasone, digoxin, nicardipine, rhodamine B, paclitaxel, vinblastine, vincristine, and valinomycin, were examined (Table 1). The effects of cholesterol on K_m and V_{max} values of MDR1 ATPase activity differ from one drug to another as discussed later in the Discussion section.

Effect of cholesterol on steroid-stimulated ATPase activity of MDR1

We initially presumed that cholesterol would compete with dexamethasone at the shared binding site and increase the

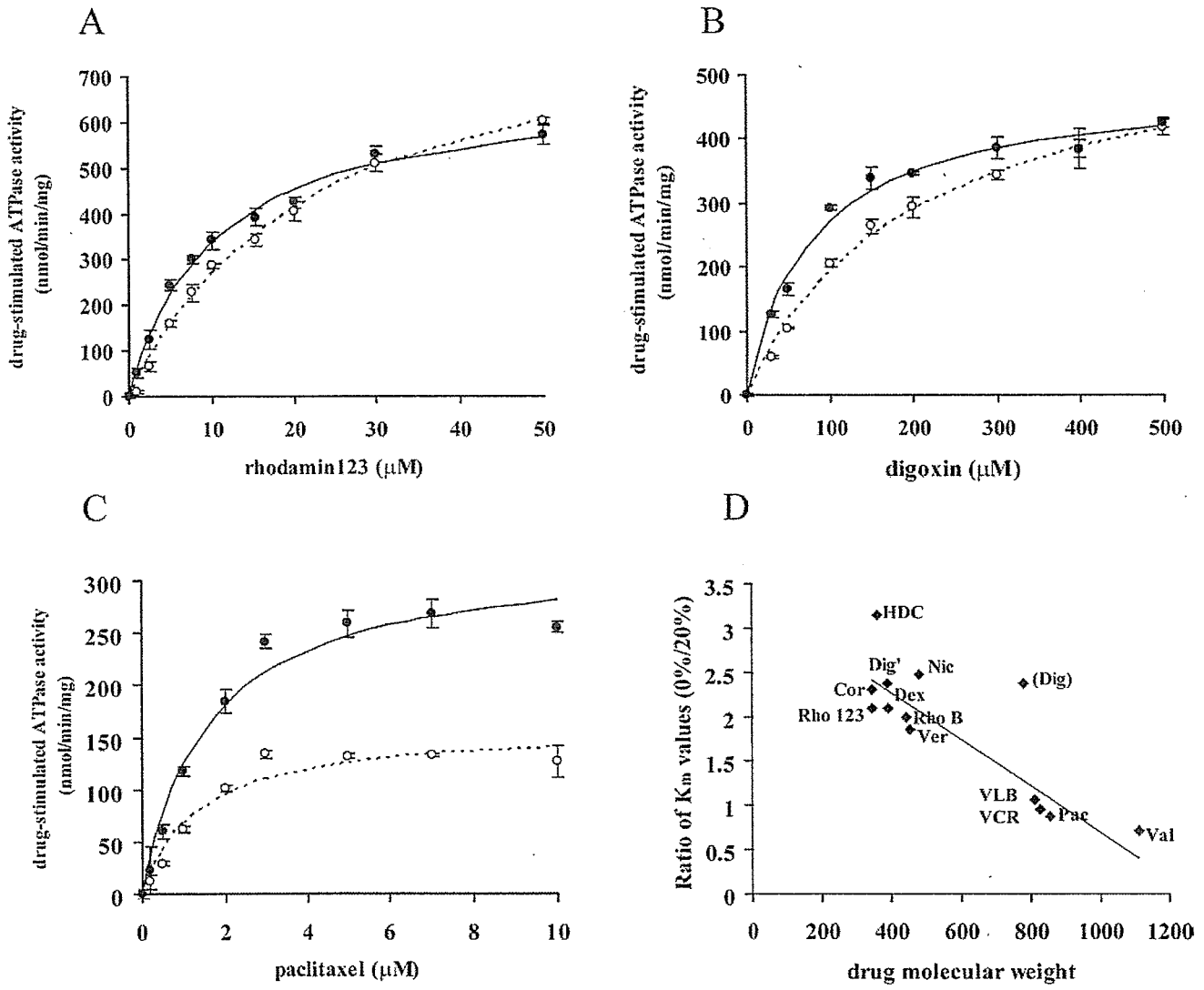

Figure 6 The effect of cholesterol on drug-stimulated ATPase activity

Purified MDR1 reconstituted in liposomes containing 0 % (open symbols) or 20 % (filled symbols) cholesterol was reacted in the presence of various concentrations of drugs. (**A**) Rhodamine 123, (**B**) digoxin, and (**C**) paclitaxel. Experiments were performed in triplicate and means ± S.D. are shown. After subtraction of the basal (without drug) activity, data were fitted to the Michaelis–Menten equation and K_m and V_{0max} values were extracted. Lines represent calculated best-fit curves. (**D**) Relationship between the ratio of K_m values in the absence and presence of 20 % (w/w) cholesterol and the molecular masses of drugs. The line represents the best fit linear regression ($r^2 = 0.8075$; excluding the points for digoxin). Rho123, rhodamine 123; Cor, corticosterone; HDC, hydrocortisone; Dex, dexamethasone; Dig', aglycon form of digoxin; RhoB, rhodamine B; Ver, verapamil; Nic, nicardipine; Dig; digoxin; VLB, vinblastine; VCR, vincristine; Pac, paclitaxel; Val, valinomycin.

K_m value for dexamethasone. However, as shown in Table 1, cholesterol decreased the K_m value for dexamethasone, indicating that the binding site for cholesterol is different from that for dexamethasone. To further examine the effect of cholesterol, we analysed effects on the ATPase activity of MDR1 stimulated by corticosterone and hydrocortisone (Figure 7). K_m values for both corticosterone and hydrocortisone decreased from 485 μM to 210 μM and from 1498 μM to 475 μM respectively when MDR1 was reconstituted in liposomes containing 20 % cholesterol.

Effects of sterols on paclitaxel-stimulated ATPase activity of MDR1

Table 2 shows the effects of various sterols on the paclitaxel-stimulated ATPase activity of MDR1. Stigmasterol, sitosterol and campesterol as well as cholesterol increased the V_{max} value significantly. Ergosterol increased the V_{max} value slightly. On the other hand, all of these sterols decreased the K_m value and increased the V_{max} value of the rhodamine B-stimulated ATPase activity of MDR1 as efficiently as cholesterol (results not shown). These results also suggest that the action of sterols is drug specific.

Effect of cholesterol depletion on drug-stimulated ATPase activity of MDR1 in mammalian cells

It has been reported that the depletion of membrane cholesterol significantly reduces the MDR1-mediated transport activity [23,26]. To investigate the role of cholesterol in the MDR1 ATPase activity in mammalian cells, we expressed MDR1 in FreeStyle HEK-293F cells and analysed the effect of cholesterol depletion on the verapamil-stimulated ATPase activity. With the depletion of cholesterol with 10 mM MβCD, the K_m value for verapamil

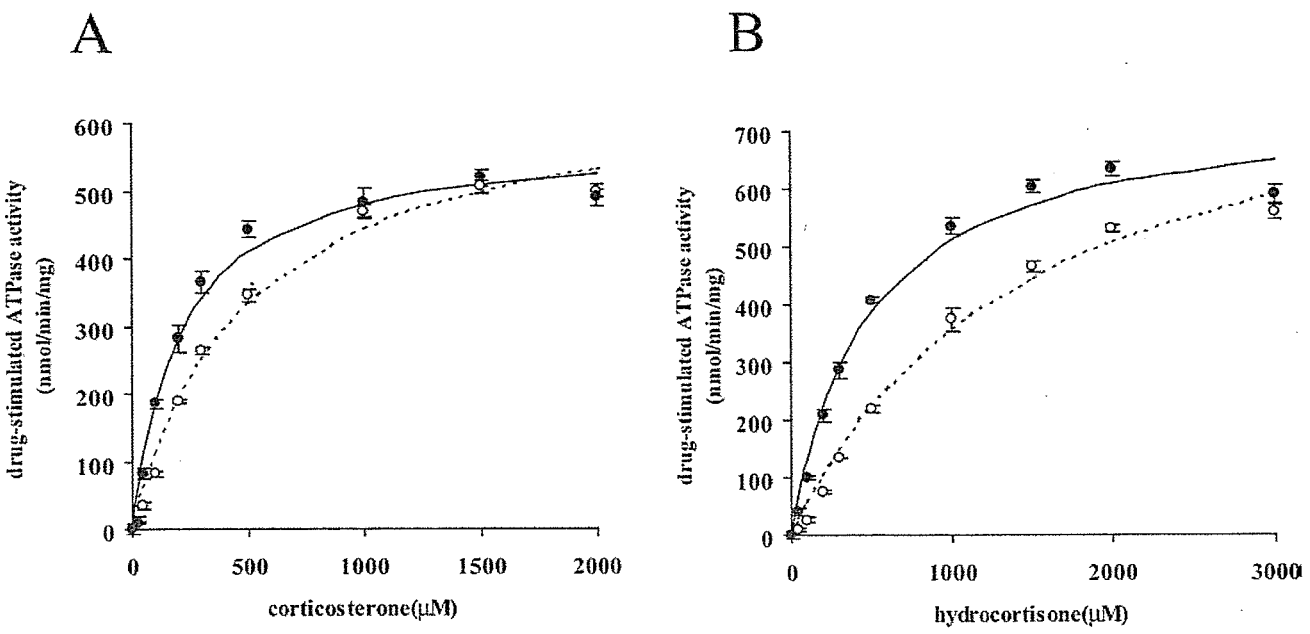

Figure 7 Effects of cholesterol on corticosterone- and hydrocortisone-stimulated ATPase activity

Purified MDR1 reconstituted in liposomes containing 0% (open symbols) or 20% (filled symbols) cholesterol was reacted in the presence of corticosterone (**A**) or hydrocortisone (**B**). Experiments were performed in triplicate and means ± S.D. are shown. Lines represent calculated best-fit curves.

shifted from 3.2 ± 0.8 μM to 4.4 ± 0.2 μM, although the V_{max} value was not reduced. This result suggests that the amount of cholesterol also affects the K_m value for drugs of MDR1 in native membranes, as observed in reconstituted liposomes.

DISCUSSION

The results obtained in the present study demonstrate that cholesterol in membranes interacts directly with MDR1 and affects not only the basal ATPase activity but also the drug-stimulated ATPase activity of MDR1. Cholesterol affects both drug-binding (K_m) and turnover of ATP hydrolysis (V_{max}) of the purified human MDR1 reconstituted in liposomes. The effects of cholesterol differ from one drug to another and can be classified into five types depending on changes of kinetic parameters (Table 1). Type I involves rhodamine 123, dexamethasone, verapamil, nicardipine and digoxin: the K_m decreases in the presence of 20% cholesterol, but the V_{max} is little affected. Type II involves rhodamine B: the K_m decreases and the V_{max} increases in the presence of cholesterol. Type III involves vinblastine and vincristine: neither the K_m nor the V_{max} is affected greatly. Type IV involves paclitaxel: the K_m is not much affected and the V_{max} increases in the presence of cholesterol. Type V involves valinomycin: the K_m increases in the presence of cholesterol and the V_{max} is little affected.

The effects of cholesterol on the K_m were drug-specific. When the ratio of the K_m of each drug in the absence and presence of 20% cholesterol was plotted against the molecular mass of that drug, a strong correlation was found between them (Figure 6D). At first glance, digoxin did not fit the correlation, but when the aglycon form of digoxin (molecular mass 390 Da) was plotted on the graph, it fitted well. The binding affinity of drugs with a small molecular mass, between 350 and 500 Da, increased in the presence of 20% cholesterol, and these drugs (rhodamine 123, dexamethasone, verapamil, nicardipine, digoxin, corticosterone, hydrocortisone and rhodamine B) are categorized into type I and type II (Table 1, Figure 6D). The binding affinity of drugs with a molecular mass of between 800 and 900 Da is not affected much by cholesterol, and these drugs (vinblastine, vincristine and paclitaxel) are categorized into type III and type IV. The binding affinity of valinomycin (type V), whose molecular mass is over 1000 Da, decreased in the presence of 20% cholesterol.

The effects of cholesterol might possibly arise indirectly, secondary to changes in the properties of the proteoliposomes such as permeability of the drugs or fluidity of the lipid bilayer. However, there are no correlations between hydrophobicity (logP values) of drugs and the effects of cholesterol on either the K_m or V_{max} values. Cholesterol exerted various effects on the K_m in a drug-specific manner as described above, suggesting that those effects were caused by a direct interaction between MDR1 and cholesterol. The effects of cholesterol on the V_{max} values were also drug-specific. The V_{max} values for rhodamine B and paclitaxel are significantly increased in the presence of 20% cholesterol, whereas those for other drugs are not (Table 1). Moreover, the effects on V_{max} values of paclitaxel-stimulated ATPase activity are sterol-specific (Table 2). If the effects are thoroughly indirect, effects of cholesterol on drug-stimulated ATPase activity are expected to be observed for all the drugs. These results suggest that cholesterol affects the function of MDR1 by interacting with MDR1 directly, at least in part.

Modok et al. [35] showed that cholesterol alone does not alter the binding affinity for both nicardipine (molecular mass 480 Da) and XR9576 (molecular mass 647 Da). While these authors purified these proteins from drug-resistant Chinese-hamster ovary cells, in the present study we expressed and purified MDR1 in insect cells whose cholesterol content is quite low compared with that of mammalian cells [36]. This might affect the amount of cholesterol retained by the purified protein, which may cause the difference in the effects of exogenously added cholesterol.

The strong correlation between the effect of cholesterol on the K_m for drugs and their molecular masses suggests that the primary

effect of cholesterol could be on the drug-binding site. MDR1 has been suggested to possess several allosterically coupled drug-binding sites [13,14,37,38] and to bind more than one drug molecule at the same time [39,40]. Cholesterol may bind directly to or allosterically affect the drug-binding site to adjust its size for the drug. Because the binding affinity of drugs with a molecular mass of between 800 and 900 Da (vinblastine, vincristine and paclitaxel) is not affected by the presence of cholesterol, the drug-binding site of MDR1 may best fit drugs with these sizes. When small drugs, with a molecular mass of 350–500 Da, bind to MDR1, cholesterol (molecular mass 386.7 Da) may fill the empty space or allosterically tighten the drug-binding site and help in the recognition of smaller drugs.

We have previously demonstrated that the bulkiness of side chains at the position of His^{61} and its neighbouring amino acid residues in the first transmembrane helix is important for substrate specificity [41,42]. For example, the replacement of His^{61} by amino acids with bulkier side chains increased resistance to small drugs such as colchicine and VP16, while it lowered resistance to a large drug, vinblastine. Recently, it was also suggested that the first transmembrane helix forms part of the drug-binding pocket by cross-linking experiments using a thiol-reactive analogue of verapamil [43]. These observations also suggest that the size of the drug-binding pocket is important for recognizing drugs.

The most puzzling feature of MDR1 is its recognition of drugs with various structures and molecular masses, from 300 Da to well over 1000 Da. To function as an efflux pump for various lipophilic and toxic xenobiotics, it is necessary for MDR1 to recognize them as they pass through the lipid bilayer. Since substrate transport and ATP hydrolysis are tightly coupled, we have previously used purified human MDR1, reconstituted in liposomes, and measured the amounts of ADP released after the hydrolysis by HPLC with a titanium dioxide column [28]. Under our experimental conditions, the amount of detergent remaining in the ATPase reaction is less than 0.003 %. This concentration is below the c.m.c. values of DDM (0.0087 %), suggesting that reconstituted protein is embedded in the lipid bilayer. Moreover, the similar K_m values for verapamil in the native membrane (FreeStyle HEK-293F) and reconstituted proteoliposome suggest that the purified MDR1 is under native conditions as embedded in the plasma membrane. Inhibitors for other membrane-bound ATPases such as sodium azide and ouabain, which are necessary when membrane-bound or partially purified MDR1 is used in experiments [44,45], were not needed in the present study. These experimental conditions allowed us to examine the effect of cholesterol in the lipid bilayer on the MDR1 ATPase activity in detail. Because cholesterol is a major [about 20 % (w/w) of lipids] and important constituent of the plasma membrane [46], liposomes containing cholesterol would provide more favourable conditions for MDR1. The highly sensitive ATPase assay established in the present study will not only facilitate our understanding of the drug-recognition mechanism of MDR1 but will also be useful for screening drugs interacting with MDR1.

In summary, we have analysed the ATPase activity and cholesterol-binding of MDR1 using purified human MDR1. The results suggest that cholesterol binds directly to MDR1 and modulates substrate-recognition by MDR1. The binding affinity of drugs with a small molecular mass increased in the presence of cholesterol. Cholesterol may fill the empty space or allosterically tighten the drug-binding site and aid the recognition of smaller drugs, and facilitate the ability of MDR1 to recognize compounds with various structures and molecular masses.

We thank Dr Tatsuya Kusudo for discussions. We also thank Dr Atsushi Kodan and Dr Vassilis Koronakis for advice on experimental procedures. This work was supported by a Grant-in-aid for Scientific Research and Creative Scientific Research 15GS0301 from the Ministry of Education, Culture, Sports, Science and Technology, Ministry of Health, Labor and Welfare, Japan, the Association for the Progress of New Chemistry, and BRAIN (the Bio-oriented Technology Research Advancement Institution).

REFERENCES

1 Juliano, R. L. and Ling, V. (1976) A surface glycoprotein modulating drug permeability in Chinese hamster ovary cell mutants. Biochim. Biophys. Acta. **455**, 152–162
2 Ueda, K., Cardarelli, C., Gottesman, M. M. and Pastan, I. (1987) Expression of a full-length cDNA for the human 'MDR1' gene confers resistance to colchicine, doxorubicin and vinblastine. Proc. Natl. Acad. Sci. U.S.A. **84**, 3004–3008
3 Gottesman, M. M. and Pastan, I. (1993) Biochemistry of multidrug resistance mediated by the multidrug transporter. Annu. Rev. Biochem. **62**, 385–427
4 Gottesman, M. M., Pastan, I. and Ambudkar, S. V. (1996) P-glycoprotein and multidrug resistance. Curr. Opin. Genet. Dev. **6**, 610–617
5 Sparreboom, A., van Asperen, J., Mayer, U., Schinkel, A. H., Smit, J. W., Meijer, D. K., Borst, P., Nooijen, W. J., Beijnen, J. H. and van Tellingen, O. (1997) Limited oral bioavailability and active epithelial excretion of paclitaxel (Taxol) caused by P-glycoprotein in the intestine. Proc. Natl. Acad. Sci. U.S.A. **94**, 2031–2035
6 Ambudkar, S. V., Dey, S., Hrycyna, C. A., Ramachandra, M., Pastan, I. and Gottesman, M. M. (1999) Biochemical, cellular and pharmacological aspects of the multidrug transporter. Annu. Rev. Pharmacol. Toxicol. **39**, 361–398
7 Greiner, B., Eichelbaum, M., Fritz, P., Kreichgauer, H. P., von Richter, O., Zundler, J. and Kroemer, H. K. (1999) The role of intestinal P-glycoprotein in the interaction of digoxin and rifampin. J. Clin. Invest. **104**, 147–153
8 Chen, C. J., Chin, J. E., Ueda, K., Clark, D. P., Pastan, I., Gottesman, M. M. and Roninson, I. B. (1986) Internal duplication and homology with bacterial transport proteins in the mdr1 (P-glycoprotein) gene from multidrug-resistant human cells. Cell. **47**, 381–389
9 Urbatsch, I. L., Sankaran, B., Bhagat, S. and Senior, A. E. (1995) Both P-glycoprotein nucleotide-binding sites are catalytically active. J. Biol. Chem. **270**, 26956–26961
10 Takada, Y., Yamada, K., Taguchi, Y., Kino, K., Matsuo, M., Tucker, S. J., Komano, T., Amachi, T. and Ueda, K. (1998) Non-equivalent cooperation between the two nucleotide-binding folds of P-glycoprotein. Biochim. Biophys. Acta. **14**, 131–136
11 Ambudkar, S. V., Cardarelli, C. O., Pashinsky, I. and Stein, W. D. (1997) Relation between the turnover number for vinblastine transport and for vinblastine-stimulated ATP hydrolysis by human P-glycoprotein. J. Biol. Chem. **272**, 21160–21166
12 Eytan, G. D., Regev, R. and Assaraf, Y. G. (1996) Functional reconstitution of P-glycoprotein reveals an apparent near stoichiometric drug transport to ATP hydrolysis. J. Biol. Chem. **271**, 3172–3178
13 Martin, C., Berridge, G., Higgins, C. F., Mistry, P., Charlton, P. and Callaghan, R. (2000) Communication between multiple drug binding sites on P-glycoprotein. Mol. Pharmacol. **58**, 624–632
14 Shapiro, A. B., Fox, K., Lam, P. and Ling, V. (1999) Stimulation of P-glycoprotein-mediated drug transport by prazosin and progesterone: evidence for a third drug-binding site. Eur. J. Biochem. **259**, 841–850
15 Loo, T. W., Bartlett, M. C. and Clarke, D. M. (2003) Methanethiosulfonate derivatives of rhodamine and verapamil activate human P-glycoprotein at different sites. J. Biol. Chem. **278**, 50136–50141
16 Loo, T. W. and Clarke, D. M. (2002) Location of the rhodamine-binding site in the human multidrug resistance P-glycoprotein. J. Biol. Chem. **277**, 44332–44338
17 Yu, L., Hammer, R. E., Li-Hawkins, J., Von Bergmann, K., Lutjohann, D., Cohen, J. C. and Hobbs, H. H. (2002) Disruption of Abcg5 and Abcg8 in mice reveals their crucial role in biliary cholesterol secretion. Proc. Natl. Acad. Sci. U.S.A. **99**, 16237–16242
18 Tanaka, A. R., Abe-Dohmae, S., Ohnishi, T., Aoki, R., Morinaga, G., Okuhira, K., Ikeda, Y., Kano, F., Matsuo, M., Kioka, N. et al. (2003) Effects of mutations of ABCA1 in the first extracellular domain on subcellular trafficking and ATP binding/hydrolysis. J. Biol. Chem. **278**, 8815–8819
19 Lee, J. Y. and Parks, J. S. (2005) ATP-binding cassette transporter A1 and its role in HDL formation. Curr. Opin. Lipidol. **16**, 19–25
20 Takahashi, K., Kimura, Y., Kioka, N., Matsuo, M. and Ueda, K. (2006) Purification and ATPase activity of human ABCA1. J. Biol. Chem. **281**, 10760–10768
21 van Helvoort, A., Smith, A. J., Sprong, H., Fritzsche, I., Schinkel, A. H., Borst, P. and van Meer, G. (1996) MDR1 P-glycoprotein is a lipid translocase of broad specificity, while MDR3 P-glycoprotein specifically translocates phosphatidylcholine. Cell. **87**, 507–517
22 Rothnie, A., Theron, D., Soceneantu, L., Martin, C., Traikia, M., Berridge, G., Higgins, C. F., Devaux, P. F. and Callaghan, R. (2001) The importance of cholesterol in maintenance of P-glycoprotein activity and its membrane perturbing influence. Eur. Biophys. J. **30**, 430–442

23 Gayet, L., Dayan, G., Barakat, S., Labialle, S., Michaud, M., Cogne, S., Mazane, A., Coleman, A. W., Rigal, D. and Baggetto, L. G. (2005) Control of P-glycoprotein activity by membrane cholesterol amounts and their relation to multidrug resistance in human CEM leukemia cells. Biochemistry. **44**, 4499–4509
24 Garrigues, A., Escargueil, A. E. and Orlowski, S. (2002) The multidrug transporter, P-glycoprotein, actively mediates cholesterol redistribution in the cell membrane. Proc. Natl. Acad. Sci. U.S.A. **99**, 10347–10352
25 Troost, J., Albermann, N., Emil Haefeli, W. and Weiss, J. (2004) Cholesterol modulates P-glycoprotein activity in human peripheral blood mononuclear cells. Biochem. Biophys. Res. Commun. **316**, 705–711
26 Troost, J., Lindenmaier, H., Haefeli, W. E. and Weiss, J. (2004) Modulation of cellular cholesterol alters P-glycoprotein activity in multidrug-resistant cells. Mol. Pharmacol. **66**, 1332–1339
27 Kioka, N., Tsubota, J., Kakehi, Y., Komano, T., Gottesman, M. M., Pastan, I. and Ueda, K. (1989) P-glycoprotein gene (MDR1) cDNA from human adrenal: normal P-glycoprotein carries Gly^{185} with an altered pattern of multidrug resistance. Biochem. Biophys. Res. Commun. **162**, 224–231
28 Kimura, Y., Shibasaki, S., Morisato, K., Ishizuka, N., Minakuchi, H., Nakanishi, K., Matsuo, M., Amachi, T., Ueda, M. and Ueda, K. (2004) Microanalysis for MDR1 ATPase by high-performance liquid chromatography with a titanium dioxide column. Anal. Biochem. **326**, 262–266
29 Takeuchi, K., Yokogawa, M., Matsuda, T., Sugai, M., Kawano, S., Kohno, T., Nakamura, H., Takahashi, H. and Shimada, I. (2003) Structural basis of the KcsA K(+) channel and agitoxin2 pore-blocking toxin interaction by using the transferred cross-saturation method. Structure. **11**, 1381–1392
30 Hayward, R. D., Cain, R. J., McGhie, E. J., Phillips, N., Garner, M. J. and Koronakis, V. (2005) Cholesterol binding by the bacterial type III translocon is essential for virulence effector delivery into mammalian cells. Mol. Microbiol. **56**, 590–603
31 Radhakrishnan, A., Sun, L. P., Kwon, H. J., Brown, M. S. and Goldstein, J. L. (2004) Direct binding of cholesterol to the purified membrane region of SCAP: mechanism for a sterol-sensing domain. Mol. Cell. **15**, 259–268
32 Chifflet, S., Torriglia, A., Chiesa, R. and Tolosa, S. (1988) A method for the determination of inorganic phosphate in the presence of labile organic phosphate and high concentrations of protein: application to lens ATPases. Anal. Biochem. **168**, 1–4
33 Muller, M., Bakos, E., Welker, E., Varadi, A., Germann, U. A., Gottesman, M. M., Morse, B. S., Roninson, I. B. and Sarkadi, B. (1996) Altered drug-stimulated ATPase activity in mutants of the human multidrug resistance protein. J. Biol. Chem. **271**, 1877–1883
34 Loo, T. W. and Clarke, D. M. (1999) Identification of residues in the drug-binding domain of human P-glycoprotein: analysis of transmembrane segment 11 by cysteine-scanning mutagenesis and inhibition by dibromobimane. J. Biol. Chem. **274**, 35388–35392
35 Modok, S., Heyward, C. and Callaghan, R. (2004) P-glycoprotein retains function when reconstituted into a sphingolipid- and cholesterol-rich environment. J. Lipid Res. **45**, 1910–1918
36 Gimpl, G., Klein, U., Reilander, H. and Fahrenholz, F. (1995) Expression of the human oxytocin receptor in baculovirus-infected insect cells: high-affinity binding is induced by a cholesterol-cyclodextrin complex. Biochemistry. **34**, 13794–13801
37 Sharom, F. J., Yu, X., DiDiodato, G. and Chu, J. W. (1996) Synthetic hydrophobic peptides are substrates for P-glycoprotein and stimulate drug transport. Biochem. J. **320**, 421–428
38 Maki, N., Hafkemeyer, P. and Dey, S. (2003) Allosteric modulation of human P-glycoprotein: inhibition of transport by preventing substrate translocation and dissociation. J. Biol. Chem. **278**, 18132–18139
39 Dey, S., Ramachandra, M., Pastan, I., Gottesman, M. M. and Ambudkar, S. V. (1997) Evidence for two nonidentical drug-interaction sites in the human P-glycoprotein. Proc. Natl. Acad. Sci. U.S.A. **94**, 10594–10599
40 Loo, T. W., Bartlett, M. C. and Clarke, D. M. (2003) Simultaneous binding of two different drugs in the binding pocket of the human multidrug resistance P-glycoprotein. J. Biol. Chem. **278**, 39706–39710
41 Taguchi, Y., Morishima, M., Komano, T. and Ueda, K. (1997) Amino acid substitutions in the first transmembrane domain (TM1) of P-glycoprotein that alter substrate specificity. FEBS Lett. **413**, 142–146
42 Taguchi, Y., Kino, K., Morishima, M., Komano, T., Kane, S. E. and Ueda, K. (1997) Alteration of substrate specificity by mutations at the His^{61} position in predicted transmembrane domain 1 of human MDR1/P-glycoprotein. Biochemistry. **36**, 8883–8889
43 Loo, T. W., Bartlett, M. C. and Clarke, D. M. (2006) Transmembrane segment 1 of human P-glycoprotein contributes to the drug binding pocket. Biochem. J. **396**, 537–545
44 Sarkadi, B., Price, E. M., Boucher, R. C., Germann, U. A. and Scarborough, G. A. (1992) Expression of the human multidrug resistance cDNA in insect cells generates a high activity drug-stimulated membrane ATPase. J. Biol. Chem. **267**, 4854–4858
45 al-Shawi, M. K. and Senior, A. E. (1993) Characterization of the adenosine triphosphatase activity of Chinese hamster P-glycoprotein. J. Biol. Chem. **268**, 4197–4206
46 Sprong, H., van der Sluijs, P. and van Meer, G. (2001) How proteins move lipids and lipids move proteins. Nat. Rev. Mol. Cell. Biol. **2**, 504–513

Received 27 April 2006/3 October 2006; accepted 10 October 2006
Published as BJ Immediate Publication 10 October 2006, doi:10.1042/BJ20060632

Original Paper

nephron Physiology

Nephron Physiol 2006;102:p51–p60
DOI: 10.1159/000089682

Received: March 10, 2005
Accepted: July 20, 2005
Published online: November 10, 2005

Effect of Trimethoprim-Sulfamethoxazole on Na^+ and K^+ Transport Properties in the Rabbit Cortical Collecting Duct Perfused in vitro

Shigeaki Muto Shuichi Tsuruoka Yukio Miyata Akio Fujimura Eiji Kusano

Departments of Nephrology and Clinical Pharmacology, Jichi Medical School, Minamikawachi, Kawachi, Tochigi, Japan

Key Words
Trimethoprim · Sulfamethoxazole · Hyperkalemia · Rabbit cortical collecting duct

Abstract
Background: In this study, the membrane mechanisms of hyperkalemia caused by trimethoprim-sulfamethoxazole (TMP-SMX) combination antibiotics were assessed in the cortical collecting duct (CCD). ***Methods:*** We used the microelectrode technique and flux measurements, and examined the effects of TMP and SMX on electrical properties of the apical and basolateral membranes in the rabbit CCD perfused in vitro. ***Results:*** TMP in the lumen caused increases in apical membrane voltage, fractional apical membrane resistance (fR_A), and transepithelial resistance (R_T), all effects which were completely inhibited by luminal amiloride, but not by luminal Ba^{2+}. The luminal TMP inhibited both net Na^+ reabsorption and K^+ secretion in the CCD. TMP in the bath slightly but significantly depolarized transepithelial voltage and basolateral membrane voltage without influencing fR_A or R_T. SMX in the lumen or bath had no effect on barrier voltages or resistances. ***Conclusion:*** TMP mainly acts on the apical membrane of the CCD, inhibits the amiloride-sensitive macroscopic Na^+ conductance in this membrane, and thereby decreases the net driving force for K^+ exit across the membrane, resulting in an inhibition of K^+ secretion. SMX in the lumen or bath had no effect on the CCD.

Introduction

The trimethoprim-sulfamethoxazole (TMP-SMX) combination antibiotics is an extremely common medication given for treatment of a variety of infections. The adverse effect of hyperkalemia has been reported in acquired immunodeficiency syndrome patients 7–10 days after the start of high doses of TMP-SMX therapy for treatment of *Pneumocystitis carinii* pneumonia [1–3] and in hospitalized patients treated with standard doses of TMP-SMX [4]. The hyperkalemia appears to be reversible as it ameliorates after withdrawal of the drug [1, 2].

The mechanisms for the hyperkalemia caused by TMP-SMX have not fully been understood, but the renin-angiotensin-aldosterone axis appears to be intact in most, but not all, cases [5, 6]. Fonseca et al. [7] reported that TMP inhibits Na^+ transport across the frog skin and competes with amiloride for blockade of Na^+ conductance. Velázquez et al. [8] described that TMP, when acutely infused into rats, caused a natriuresis and a fall in urinary K^+ excretion. They also observed that, in rat distal tubule perfused in vivo, addition of TMP to the luminal perfusate decreased net K^+ secretion and lumen-negative transepithelial voltage (V_T), and speculated that TMP may impair Na^+ transport in the distal tubule and reduces lumen-negative V_T by the Na^+ transport, thereby decreasing the electrical gradient favoring passive K^+ secretion. However, they did not directly demonstrate it, because TMP had no effect on net Na^+ reabsorption in the distal tubule [8]. Because the distal tubule is composed of

KARGER
Fax +41 61 306 12 34
E-Mail karger@karger.ch
www.karger.com

1660–2137/06/1024–0051$23.50/0

Accessible online at:
www.karger.com/nep

Dr. Shigeaki Muto
Department of Nephrology, Jichi Medical School
Minamikawachi, Kawachi
Tochigi 329-0498 (Japan)
Tel. +81 285 58 7346, Fax +81 285 44 4869, E-Mail smuto@jichi.ac.jp

heterogeneous cells such as distal convoluted tubule cells, connecting tubule cells, principal collecting duct (CD) cells, and α-intercalated cells [9], which cell(s) contribute(s) to the TMP-induced electrical changes remains unknown. In an A6 cell line derived from *Xenopus laevis* distal nephron, a model of mammalian cortical collecting duct (CCD) CD cell, Choi et al. [1] have shown that the apical TMP, but not the basolateral TMP, inhibited amiloride-sensitive short circuit current. Schlanger et al. [10] applied cell-attached patch clamp techniques to the A6 cell monolayers and reported that TMP acted from the apical membrane, and inhibited highly selective Na^+ channel activity. However, it is not known whether TMP actually inhibits macroscopic Na^+ conductance at the apical membrane of the intact mammalian CD cell and reduces net Na^+ reabsorption and K^+ secretion in the CCD. It is also possible that TMP may interact with SMX, and as a consequence may inhibit apical membrane Na^+ conductance. Furthermore, there is a question as to whether TMP may directly act on the apical K^+ conductance. In addition, Eiam-Ong et al. [11] reported a decrease in Na^+-K^+-ATPase activity in the rat CCD, a finding that may also be able to account for the TMP-induced hyperkalemia. However, whether TMP directly influences basolateral Na^+-K^+ pump activity in the CCD is unclear. The above-mentioned reports suggest that TMP may act on both apical and basolateral membranes of the CD cell; however, which action contributes to the TMP-induced hyperkalemia remains unknown.

Therefore, the purpose of the present study was to determine the cellular and membrane mechanisms for the TMP-SMX-induced hyperkalemia. For this purpose, we examined the effects of TMP and SMX in the lumen and bath on electrical properties in the apical and basolateral membranes of the CD cell in isolated perfused CCDs from rabbit kidneys. We also examined the effects of TMP in the lumen on net transepithelial fluxes of Na^+ and K^+ in CCDs perfused in vitro.

Methods

Isolation and Perfusion of Tubules

Japanese female white rabbits (1.5–2.5 kg) were maintained on a standard rabbit chow and tap water ad libitum. The animals were anesthetized with intravenous sodium pentobarbital (35 mg/kg) and both kidneys were removed. Thin slices (1–2 mm) were cut from the coronal section of each kidney and transferred to a dish containing dissecting solution composed of (in m*M*): 14 KCl, 44 K_2HPO_4, 14 KH_2PO_4, 9 $NaHCO_3$ and 160 sucrose, a medium that had been shown to improve the quality of the kidney tissue [12–16]. The CCD was dissected and transferred to a bath chamber mounted on an inverted microscope (Diaphot; Nikon, Tokyo, Japan). Methods used to perfuse the CCD have been described previously in our laboratory [12–15]. Briefly, after suspending the tubule between two pipettes, the lumen was perfused at a rate exceeding 20 nl/min. The distal end of the CCD was held in a collecting pipette coated with unpolymerized Sylgard 184 (Dow Corning Corp., Midland, Mich., USA). The volume of the bath chamber was ~100 μl to permit rapid exchange of different bath solutions within 5 s. The bath solution flowed by gravity at a rate of 5–15 ml/min from the reservoirs through a water jacket to stabilize the bath temperature at XXX.

Electrical Measurements

The transepithelial and cellular electrical potentials were measured using methods described previously [12–15]. Briefly, transepithelial voltage (V_T) was measured through the perfusion pipette, which was connected to one channel of a dual electrometer (Duo 773; W-P Instruments, Inc., Sarasota, Fla., USA) with a 3 *M* KCl-3% agar bridge and a calomel half-cell electrode. Bathing fluid was also connected through a 3 *M* KCl-3% agar bridge connected to another calomel half-cell electrode. Constant-current pulses (ΔI) (50 nA, 1 s in duration, and 10-second intervals) were injected into the tubule lumen via the perfusion pipette connected to a pulse generator (SEN-3301; Nihon Kohden, Tokyo, Japan). The voltage deflection at the perfusion end of the tubule (ΔV_P) was recorded via 3 *M* KCl-3% agar bridge and the electrometer noted above. The voltage deflection at the distal end of the tubule (ΔV_D) was also measured via a 3 *M* KCl-3% agar bridge inserted into the collecting pipette, which was connected to another electrometer (MEZ-7200; Nihon Kohden). The basolateral membrane voltage (V_B) was measured with 0.5 *M* KCl-filled microelectrodes, which were fabricated from borosilicate glass capillaries (GD-1.5; 1.5 mm OD, 1.0 mm ID; Narishige Scientific Laboratory, Tokyo, Japan) by using a vertical puller (PE-2; Narishige Scientific Laboratory). They were fixed to a microelectrode holder containing an Ag-AgCl pellet and connected to another channel of a dual electrometer (Duo 773; W-P Instruments). To impale a tubular cell, a microelectrode was positioned against the basolateral membrane with a hydraulic micromanipulator (WR-6; Narishige Scientific Laboratory) fixed to the stage of a microscope (Diaphoto, Nikon). The microelectrode was advanced into the cell by tapping the air-cushioned table. Both V_T and V_B were referenced to the bath and were recorded on a four-pen chart recorder (R64; Rikadenki, Tokyo, Japan). The electrical potential difference across the apical membrane (V_A) was calculated as $V_A = V_T - V_B$. The length constant (λ) was determined by

$$L/\lambda = \cosh^{-1} (\Delta V_P/\Delta V_D),$$

where L is the tubular length. R_T is obtained from the following equation [12–15]:

$$R_T = 2\pi r\lambda (\Delta V_P/\Delta I) \tanh (L/\lambda),$$

where r is the optical radius of the tubule. The fractional apical membrane resistance (fR_A) was estimated as the following equation [12–15]:

$$fR_A = (\Delta V_x - \Delta V_B)/\Delta V_x,$$

where ΔV_B and ΔV_x are the current-induced voltage deflection of the V_B and the deflection of the V_T at the point of the microelectrode impalement, respectively. The ΔV_x was estimated as

$$\Delta V_x = \Delta V_P \cosh (x/\lambda - L/\lambda)/\cosh (L/\lambda),$$

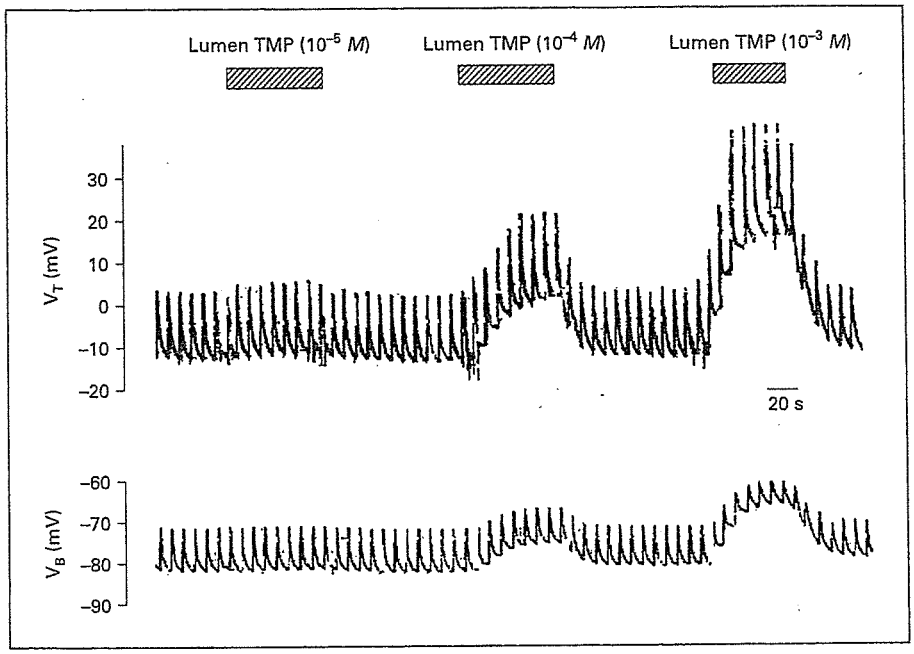

Fig. 1. Typical tracings showing effects of TMP at 10^{-5}, 10^{-4}, and 10^{-3} *M* in the lumen on V_T and V_B in the CCD. Voltage spikes are due to 50 nA constant-current pulses at 10-second intervals.

where x is the distance from the tip of the perfusion pipette to the point of cell impalement. The electrical radius calculated from the volume resistivity of the luminal perfusate and core resistance coincided with the optical radius within the range of variability of the measurements.

In the present experiments, only CD cells in the rabbit CCD were impaled, using methods of identification previously described [12–15].

Measurements of Net Transepithelial Na^+ and K^+ Fluxes

Net transepithelial water flux (J_V, nl/mm/min) was calculated as $J_V = V_0 (C^*_o/C^*_i - 1)/L$, where V_0 is the fluid collected rate (nl/min), L is the tubular length (mm), C^*_o and C^*_i are concentrations of ^{14}C-methoxy inulin (New England Nuclear, Boston, Mass., USA) of the collected fluid and the luminal perfusate, respectively [16, 17]. The values of J_V greater than ± 0.1 nl/mm/min were assumed to represent water movement, including mechanical leaks, and were discarded. Net transepithelial fluxes of Na^+ and K^+ were determined by measuring concentrations of the luminal perfusate and collected fluid with a continuous flow fluorometer (Nanoflo; W-P Instruments) [17] and an ultramicro flame photometer (AFA-707-D; APEL, Saitama, Japan) [16], respectively. The net transepithelial fluxes of the solute X (J_X, pEq/mm/min) were calculated according to the equation: $J_X = ([X]_i - [X]_o) V_o/L$, where $[X]_i$ and $[X]_o$ are concentrations of the solute X in the luminal perfusate and the collected fluid, respectively. Negative value of J_X indicates net secretion. For the flux studies, the luminal flow rate was adjusted to ~7 nl/min by regulating the hydrostatic perfusion pressure. Each reported flux represents the difference between three paired samples of the luminal perfusate and collected fluid with each sample measured in triplicate.

Solutions and Materials

The composition of the bathing and luminal solution used in this study was as follows (in m*M*): 110 NaCl, 5 KCl, 25 $NaHCO_3$, 0.8 Na_2HPO_4, 0.2 NaH_2PO_4, 10 sodium acetate, 1.8 $CaCl_2$, 1.0 $MgCl_2$, 8.3 *d*-glucose, and 5 *L*-alanine. The pH of the solution was maintained at 7.4 by bubbling with 95% O_2 and 5% CO_2 gas, and the osmolality of the solution was between 285 and 295 mosm/kg H_2O.

Amiloride (Sigma Chemicals, St. Louis, Mo., USA) was added to the luminal perfusate to achieve a final concentration of 50 μ*M*. $BaCl_2$ was used in the lumen at a final concentration of 2 m*M*. TMP, which was supplied by Shionogi & Co., Ltd. (Osaka, Japan), and SMX (Sigma) were dissolved in DMSO at 0.1% final concentrations. Equivalent concentrations of vehicle were added as a control for individual protocols.

Statistics

Data are shown as means ± SEM, and paired Student's t test was used to determine the significance of difference between successive measurements carried out on the same tubules. Statistical significance was taken as $p < 0.05$.

Results

General Data

The CCD segments used in this study had an average length of 904.8 ± 36.4 μm (n = 23). The optical inside diameter of these tubules was 26.8 ± 0.6 μm (n = 23). The V_T averaged −8.5 ± 0.8 mV (n = 23). The mean values of the R_T and length constant were 114.5 ± 2.0 Ω cm^2

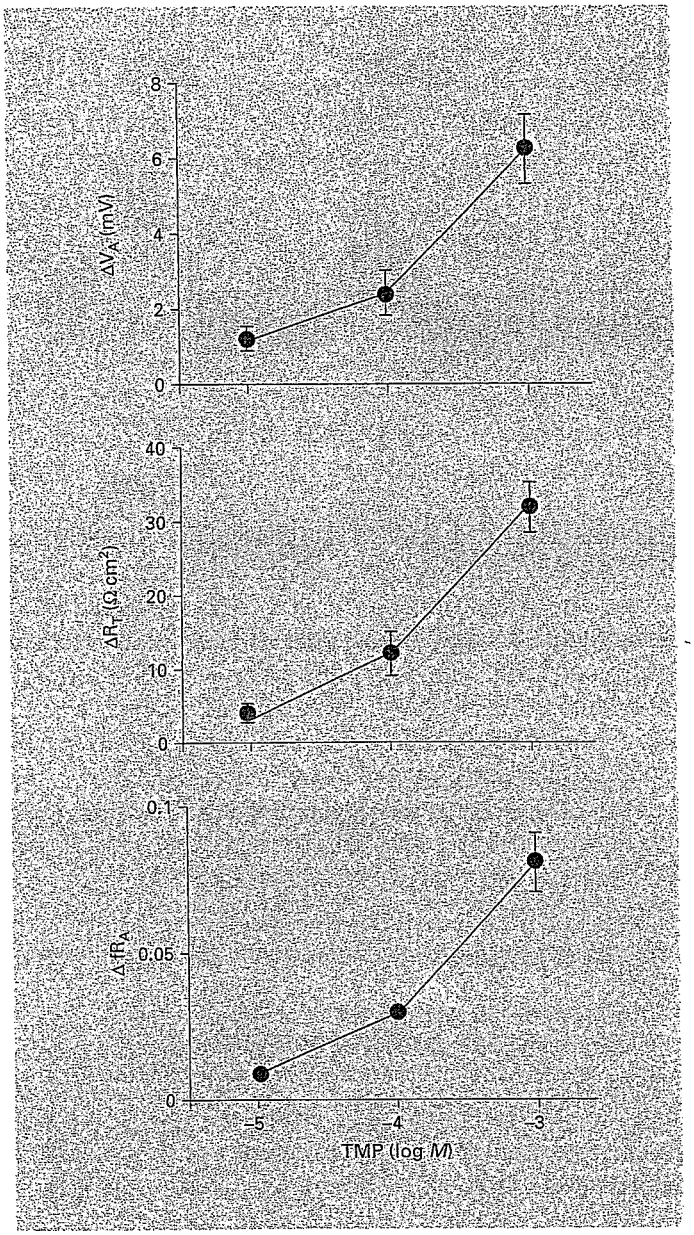

(n = 23) and 355.6 ± 13.3 μm (n = 23), respectively. These general data confirmed well with our previous reports [12–15].

Effect of TMP and SMX in the Lumen on Electrical Properties of the CD Cell

At first, we examined whether TMP acts directly on the apical membrane of the CD cell. For this purpose, we added TMP at 10^{-5}, 10^{-4} and 10^{-3} *M* to the luminal perfusate, and measured barrier voltages and resistances in the CCD. Figure 1 shows the effects of TMP at 10^{-5}, 10^{-4}, and 10^{-3} *M* in the lumen on V_T and V_B. Table 1 summarizes barrier voltages and resistances in the absence and presence of lumen TMP at 10^{-5} up to 10^{-3} *M*. TMP at 10^{-5} *M* in the lumen significantly depolarized V_T from –11.7 ± 2.3 to –10.5 ± 2.1 mV ($p < 0.01$) but had no effect on V_B, leading to a significant hyperpolarization of V_A from 70.9 ± 1.7 to 72.1 ± 1.8 mV ($p < 0.05$). The R_T and fR_A significantly increased from 118.7 ± 4.4 to 122.6 ± 5.1 Ω cm^2 ($p < 0.005$) and from 0.46 ± 0.09 to 0.47 ± 0.09 ($p < 0.005$), respectively. TMP at 10^{-4} *M* in the lumen rapidly depolarized V_T and V_B from –11.3 ± 2.1 to –3.1 ± 1.8 mV ($p < 0.001$) and from –81.9 ± 1.7 to –76.0 ± 1.9 mV ($p < 0.005$), respectively, resulting in a significant hyperpolarization of V_A from 70.5 ± 1.6 to 72.9 ± 1.8 mV ($p < 0.01$). The R_T and fR_A significantly increased from 118.7 ± 4.0 to 131.1 ± 6.1 Ω cm^2 ($p < 0.005$) and from 0.46 ± 0.09 to 0.49 ± 0.09 ($p < 0.001$), respectively. When TMP at 10^{-3} *M* was added to the luminal perfusate, the V_T and V_B rapidly depolarized from

Fig. 2. The concentration-response relationship for luminal addition of TMP on increases in V_A, R_T, and fR_A (ΔV_A, ΔR_T, and ΔfR_A, respectively). Each point represents mean ± SE of 8 separate experiments.

Table 1. Effects of TMP at 10^{-5}, 10^{-4}, and 10^{-3} *M* in the lumen on barrier voltages and resistances in the CCD

	Control	TMP (10^{-5} *M*)	Control	TMP (10^{-4} *M*)	Control	TMP (10^{-3} *M*)
V_T, mV	–11.7±2.3	–10.5±2.1**	–11.3±2.1	–3.1±1.8^{++}	–10.9±1.9	9.3±2.7^{++}
V_B, mV	–82.6±1.9	–82.6±1.7	–81.9±1.7	–76.0±1.9^{+}	–81.0±1.3	–67.0±2.9^{+}
V_A, mV	70.9±1.7	72.1±1.8*	70.5±1.6	72.9±1.8**	70.1±2.1	76.3±2.2^{++}
R_T, Ωcm^2	118.7±4.4	122.6±5.1^{+}	118.7±4.0	131.1±6.1^{+}	119.1±4.8	151.0±6.6^{++}
fR_A	0.46±0.09	0.47±0.09^{+}	0.46±0.09	0.49±0.09^{++}	0.45±0.09	0.53±0.09^{++}

Data are mean ± SE of 8 tubules. * $p < 0.05$, ** $p < 0.01$, $^{+}$ $p < 0.005$, $^{++}$ $p < 0.001$ compared with preceding period.

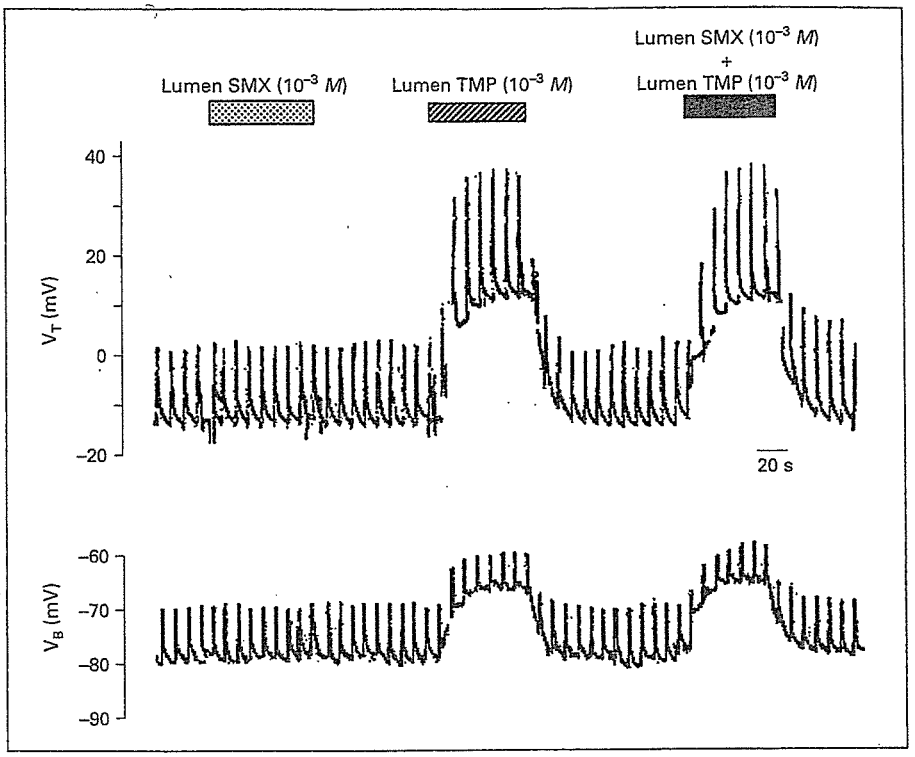

Fig. 3. Typical tracings showing effects of a separate or simultaneous addition of SMX and TMP at 10^{-3} *M* to the lumen on V_T and V_B in the CCD. Voltage spikes are due to 50 nA constant-current pulses at 10-second intervals.

Table 2. Effects of SMX and TMP in the lumen on barrier voltages and resistances in the CCD

	Control	SMX (10^{-3} *M*)	Control	TMP (10^{-3} *M*)	Control	TMP (10^{-3} *M*) + SMX (10^{-3} *M*)
V_T, mV	−10.5 ± 1.0	−10.3 ± 0.9	−10.4 ± 0.8	18.0 ± 5.5^{+}	−10.1 ± 0.9	18.3 ± 5.7^{+}
V_B, mV	−79.4 ± 3.4	−78.7 ± 3.4	−80.8 ± 3.2	−58.7 ± 3.4*	−80.7 ± 3.4	−58.3 ± 4.5^{+}
V_A, mV	68.9 ± 1.7	68.4 ± 2.9	70.4 ± 2.8	76.7 ± 2.9^{++}	70.6 ± 3.0	76.7 ± 3.4^{++}
R_T, Ωcm^2	114.3 ± 2.0	114.1 ± 2.3	112.6 ± 2.0	144.9 ± 4.1^{+}	113.6 ± 1.6	147.0 ± 4.1^{++}
fR_A	0.41 ± 0.04	0.40 ± 0.04	0.40 ± 0.04	0.48 ± 0.04^{++}	0.40 ± 0.04	0.48 ± 0.04^{++}

Data are mean ± SE of 7 tubules. * $p < 0.01$, $^{+}$ $p < 0.005$, $^{++}$ $p < 0.001$ compared with preceding period.

−10.9 ± 1.9 to 9.3 ± 2.7 mV ($p < 0.001$) and from −81.0 ± 1.3 to −67.0 ± 2.9 mV ($p < 0.005$), respectively, resulting in a significant hyperpolarization of V_A from 70.1 ± 2.1 to 76.3 ± 2.2 mV ($p < 0.001$). At this time, the R_T and fR_A significantly increased from 119.1 ± 4.8 to 151.0 ± 6.6 Ω cm^2 ($p < 0.001$) and from 0.45 ± 0.09 to 0.53 ± 0.09 ($p < 0.001$), respectively. When TMP was washed out from the luminal perfusate, the TMP-induced electrical changes were immediately eliminated. Figure 2 summarizes the concentration-response relationships for luminal addition of TMP on increases in V_A, R_T, and fR_A (ΔV_A, ΔR_T, and ΔfR_A, respectively). The ΔV_A, ΔR_T, and ΔfR_A were greater with greater concentrations of TMP.

We next examined whether SMX acts directly on the apical membrane of the CD cell. For this purpose, we added SMX at 10^{-3} *M* to the luminal perfusate, and then measured barrier voltages and resistances in the CCD. As shown in figure 3 and table 2, SMX at 10^{-3} *M* in the lumen had no effect on barrier voltages or resistances. To exclude the possibility that there may be an interaction between TMP and SMX, we simultaneously added TMP and SMX at 10^{-3} *M* in the lumen, and then observed the electrical parameters. The effects of simultaneous addi-

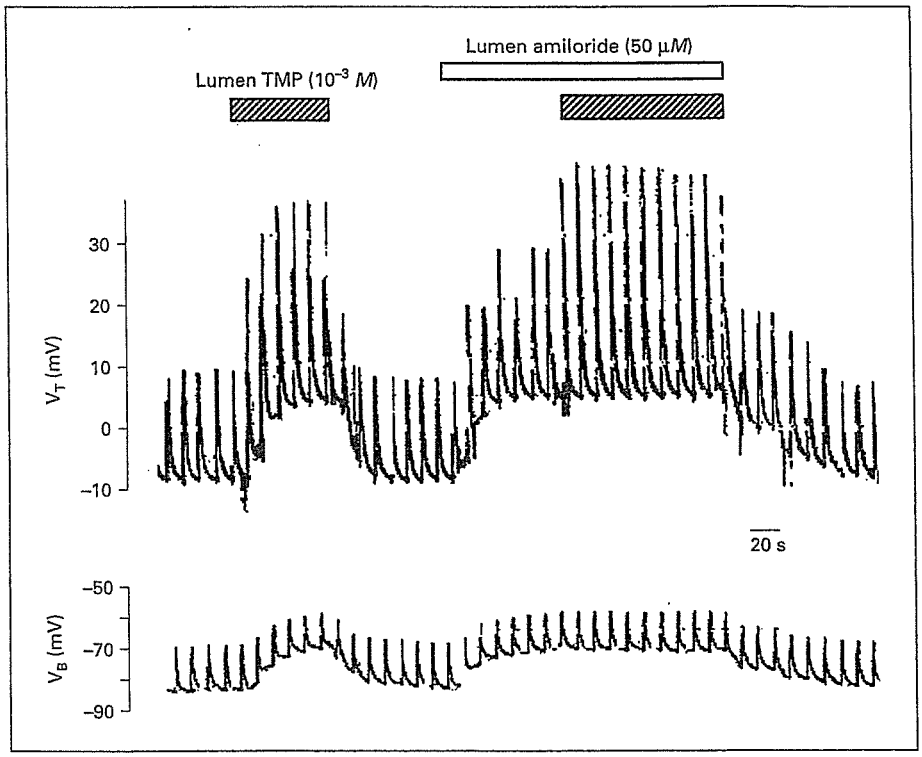

Fig. 4. Typical tracings showing effects of TMP (10^{-3} *M*) in the lumen in the absence and presence of luminal amiloride (50 μ*M*) on V_T and V_B in the CCD. Voltage spikes are due to 50 nA constant-current pulses at 10-second intervals.

Table 3. Effects of TMP in the lumen in the absence and presence of luminal amiloride on barrier voltages and resistances in the CCD

	− Amiloride		+ Amiloride	
	− TMP	+ TMP	− TMP	+ TMP
V_T, mV	−5.4 ± 0.7	5.2 ± 0.6*	6.8 ± 0.6	6.9 ± 0.8
V_B, mV	−80.8 ± 2.1	−74.5 ± 2.0*	−73.9 ± 2.7	−73.6 ± 2.8
V_A, mV	75.3 ± 2.2	81.3 ± 2.5*	80.8 ± 2.5	80.5 ± 2.6
R_T, Ωcm^2	112.3 ± 4.4	146.2 ± 6.9*	148.9 ± 8.6	148.4 ± 9.4
fR_A	0.47 ± 0.04	0.55 ± 0.05*	0.59 ± 0.04	0.58 ± 0.04

Data are mean ± SE of 9 tubules. The concentrations of TMP and amiloride were 10^{-3} *M* and 50 μ*M*, respectively. The results as shown above were serial experiments in the absence and presence of luminal amiloride. * $p < 0.001$ compared with preceding period.

tion of TMP and SMX in the lumen on barrier voltages and resistances were extremely similar to those of TMP alone in the lumen, as shown in figure 3 and table 2.

The above-mentioned findings suggest to us the possibility that only TMP in the lumen may inhibit the apical membrane Na^+ conductance in the CCD. To demonstrate this possibility, we added a Na^+ channel inhibitor amiloride (50 μ*M*) to the luminal perfusate, and then examined the effect of TMP (10^{-3} *M*) in the continued presence of luminal amiloride on CD cell. Figure 4 shows a typical tracing showing the effect of TMP in the lumen in the absence and presence of amiloride on V_T and V_B. Table 3 summarizes barrier voltages and resistances under the experimental conditions. When amiloride was added to the luminal perfusate, the lumen-negative V_T and V_B rapidly depolarized, resulting in a significant hyperpolarization of V_A by 5.5 ± 1.0 mV (n = 9). Luminal amiloride alone also significantly increased both R_T and fR_A by 32.0 ± 0.4 Ω cm^2 (n = 9) and 0.13 ± 0.02 (n = 9), respectively. These results confirm our previous observations [12, 13, 15]. When TMP was added to the lumen in the continued presence of luminal amiloride, V_T, V_B, V_A, R_T, or fR_A was no longer changed. These findings are compatible with the notion that TMP in the lumen actually inhibits amiloride-sensitive macroscopic Na^+ conductance at the apical membrane of the CD cell.

To test the possibility that TMP in the lumen may directly inhibit apical membrane K^+ conductance of the CD cell, we added Ba^{2+} (2 m*M*) to the lumen, and then observed the effect of TMP (10^{-3} *M*) in the lumen in the continued presence of luminal Ba^{2+} on electrical proper-

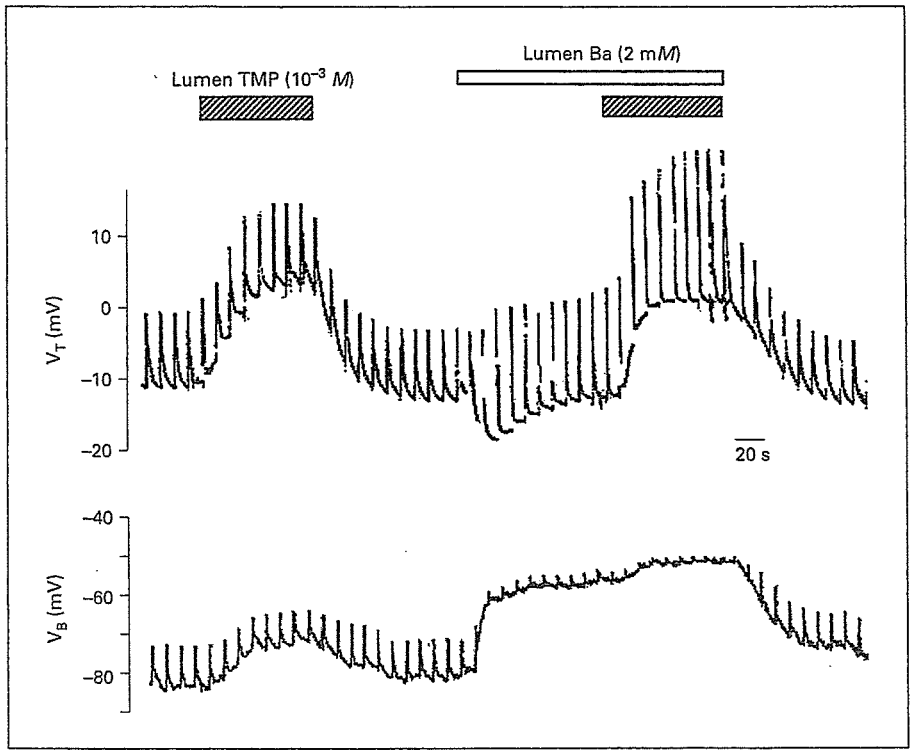

Fig. 5. Typical tracings showing effects of TMP (10^{-3} *M*) in the lumen in the absence and presence of luminal Ba^{2+} (2 m*M*) on V_T and V_B in the CCD. Voltage spikes are due to 50 nA constant-current pulses at 10-second intervals.

ties. Figure 5 shows a typical tracing showing the effect of TMP in the lumen in the absence and presence of luminal Ba^{2+} on V_T and V_B. Table 4 summarizes barrier voltages and resistances under the experimental conditions. When Ba^{2+} was added to the luminal perfusate, the lumen-negative V_T rapidly increased, and then slowly decreased to reach a new steady state level. The V_B rapidly depolarized within several seconds, and then slowly depolarized further to a new steady state level. Therefore, V_A rapidly depolarized during the first phase, and then slowly depolarized to a new steady state level. The biphasic effects of Ba^{2+} on V_T, V_B, and V_A were similar to those reported previously [13, 15]. The transient current induced by luminal addition of Ba^{2+} is due to blocking the K^+ current directed from cell to lumen. The V_T becomes more negative and the V_A becomes depolarized at first, because, after blocking the opposing K^+ current, the net current is now only composed of the Na^+ reabsorptive current. The circular Na^+ current flow produced at the apical membrane causes the V_B to depolarize. In the second phase, the Na^+ current relaxed probably due to several factors, i.e. first, a decrease in the driving force for Na^+ entry, since V_A is depolarized by ~40 mV; second, changes in intracellular ion content; and, finally, cell volume changes, because K^+ exit is eliminated by Ba^{2+} [15].

Table 4. Effects of TMP in the lumen in the absence and presence of luminal Ba^{2+} on barrier voltages and resistances in the CCD

	$-Ba^{2+}$		$+Ba^{2+}$	
	−TMP	+TMP	−TMP	+TMP
V_T, mV	−8.9 ± 1.3	7.3 ± 2.1**	−9.5 ± 1.4	4.1 ± 2.0**
V_B, mV	−83.0 ± 2.0	−73.4 ± 3.1*	−45.2 ± 3.5	−39.7 ± 4.1*
V_A, mV	73.2 ± 1.7	80.2 ± 2.2**	35.3 ± 3.3	42.9 ± 3.4**
R_T, Ωcm^2	115.0 ± 3.6	151.6 ± 4.2**	216.8 ± 10.2	252.6 ± 10.7**
fR_A	0.47 ± 0.04	0.54 ± 0.03**	0.85 ± 0.01	0.92 ± 0.01**

Data are mean ± SE of 11 tubules. The concentrations of TMP and Ba^{2+} were 10^{-3} *M* and 2 m*M*, respectively. The results as shown above were serial experiments in the absence and presence of luminal Ba^{2+}. * $p < 0.005$, ** $p < 0.001$ compared with preceding period.

Thus, both V_T and V_B slowly depolarize to a new steady state. Following addition of Ba^{2+} in the lumen, R_T increased by 101.6 ± 14.0 Ω cm^2 (n = 11) and fR_A increased by 0.38 ± 0.03 (n = 11). These findings also confirm our previous observations [13, 15]. When TMP was added to the luminal perfusate in the continued presence of luminal Ba^{2+}, both V_T and V_B further depolarized, resulting

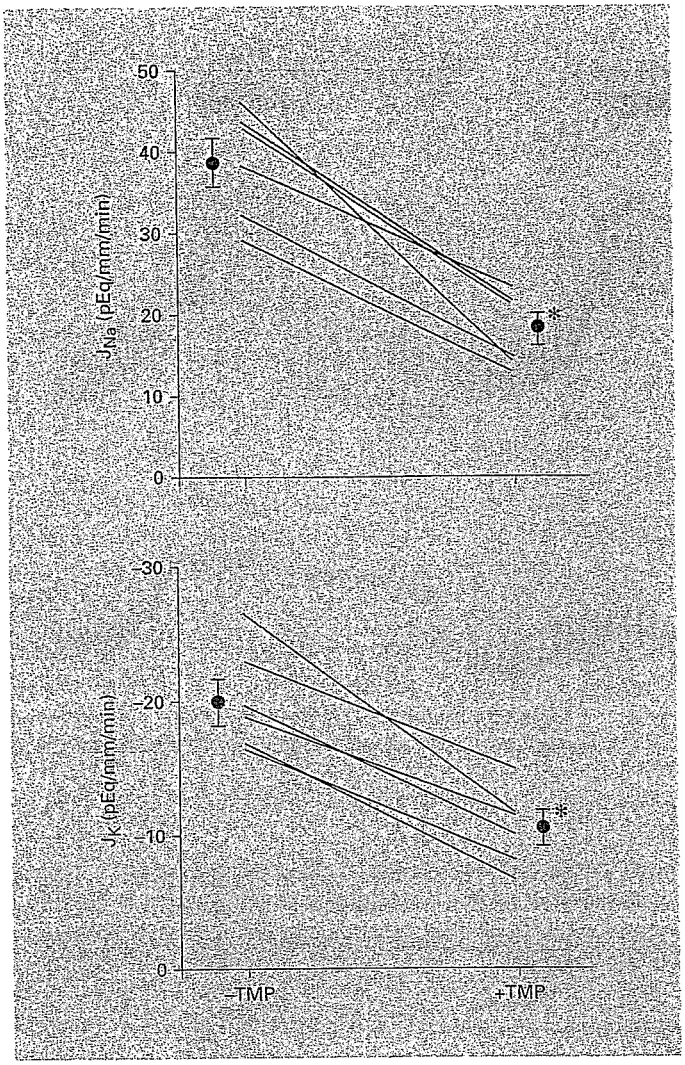

Fig. 6. Effects of TMP (10^{-3} *M*) in the lumen on net Na^+ and K^+ fluxes in the same CCD segments. Asterisk indicates that the difference is significant (*$p < 0.001$).

in a significant hyperpolarization of V_A. Under the experimental conditions, both R_T and fR_A further significantly increased. The increases in V_A or fR_A in the presence of Ba^{2+} and TMP (7.6 ± 1.1 mV or 0.07 ± 0.007, respectively) were not significantly different from those in the presence of TMP alone (7.0 ± 0.8 mV or 0.07 ± 0.009, respectively). Therefore, we concluded that TMP in the lumen did not inhibit apical membrane K^+ conductance of the CD cell at all.

We next examined whether the luminal addition of TMP actually influences net transepithelial transports of Na^+ and K^+ in the CCD perfused in vitro. The results are shown in figure 6. J_{Na} and $-J_K$ (n = 6, 18.1 ± 2.1 and 10.5 ± 1.3 pEq/mm/min, respectively) in the presence of luminal TMP at 10^{-3} *M* significantly decreased by 53.1 and 48.0% compared with those in its absence (n = 6, 38.6 ± 3.0 and 20.2 ± 1.7 pEq/mm/min, respectively).

Effect of TMP and SMX in the Bath on Electrical Properties of the CD Cell

We finally examined whether TMP and/or SMX acts directly on the basolateral membrane of the CD cell. For this purpose, we individually added TMP and SMX at 10^{-3} *M* to the bathing solution, and then observed the electrical parameters. As shown in figure 7 and table 5, TMP in the bath slightly but significantly depolarized V_T and V_B from −9.8 ± 1.1 to −8.4 ± 0.9 mV ($p < 0.001$) and from −78.5 ± 3.1 to −77.0 ± 3.3 mV ($p < 0.01$), respectively, without significant changes in R_T or fR_A, whereas SMX in the bath had no effect on barrier voltage or resistances. TMP at 10^{-4} or 10^{-5} *M* in the bath had no effect on barrier voltages or resistances (data not shown).

Discussion

In A6 cells, the apical addition of TMP has been reported to inhibit both amiloride-sensitive short circuit current [1] and Na^+ channel activity [10]. The present study used microelectrode technique and flux measurements to examine the effects of TMP and SMX on electrical properties of the apical and basolateral membranes in the rabbit CCD perfused in vitro. We demonstrated that TMP, but not SMX, mainly acts on the apical membrane of the rabbit CCD and inhibits macroscopic Na^+ conductance.

Urinary K^+ excretion is largely the result of its secretion in CD cells [reviewed in 9, 18]. This is a two-step process that involves active uptake of K^+ from blood to cell via the basolateral membrane Na^+-K^+ pump and passive diffusion from cell to lumen through a large apical membrane K^+ conductance. Apical Na^+ conductance is also involved in K^+ secretion because it not only supplies most of Na^+ for the basolateral Na^+-K^+ pump but it also depolarizes the apical membrane and thus facilitates K^+ egress into the lumen. K^+ secretion is regulated in CD cells by the supply of Na^+, the intake of K^+, by hormones such as mineralocorticoids and vasopressin, and by changes in blood pH and by many diuretics, including amiloride [9, 18].

In the current study, we found that TMP in the lumen hyperpolarized the apical membrane of the CD cell in

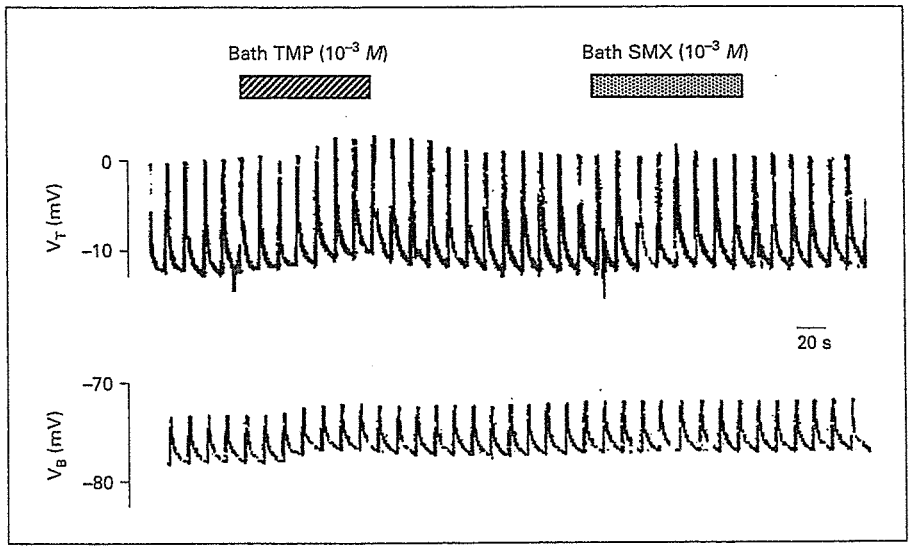

Fig. 7. Typical tracings showing effects of TMP and SMX at 10^{-3} *M* in the bath on V_T and V_B in the CCD. Voltage spikes are due to 50 nA constant-current pulses at 10-second intervals.

Table 5. Effects of TMP and SMX at 10^{-3} *M* in the bath on barrier voltages and resistances in the CCD

	Control	TMP (10^{-3} *M*)	Control	SMX (10^{-3} *M*)
V_T, mV	−9.8 ± 1.1	−8.4 ± 0.9**	−9.7 ± 1.1	−9.3 ± 1.0
V_B, mV	−78.5 ± 3.1	−77.0 ± 3.3*	−78.4 ± 2.8	−78.5 ± 2.8
V_A, mV	68.7 ± 2.5	68.6 ± 2.8	68.7 ± 2.2	69.2 ± 2.3
R_T, Ωcm^2	116.5 ± 2.8	117.4 ± 3.7	114.9 ± 3.1	114.1 ± 3.2
fR_A	0.47 ± 0.04	0.47 ± 0.04	0.47 ± 0.05	0.46 ± 0.04

Data are mean ± SE of 9 tubules. * $p < 0.01$, ** $p < 0.001$ compared with preceding period.

parallel with increases in R_T and fR_A in a concentration-dependent manner. The TMP-induced electrical changes were completely inhibited by luminal amiloride but not by luminal Ba^{2+}. TMP in the lumen also decreased both net Na^+ reabsorption and K^+ secretion in the CCD. These findings are consistent with the notion that TMP indeed acts on the apical membrane of the CD cell to inhibit the amiloride-sensitive macroscopic Na^+ conductance in the rabbit CCD. Therefore, like amiloride, TMP in the lumen causes hyperpolarization of the apical membrane, reduces the net driving force for diffusion of K^+ from cell to lumen, and thereby leads to an inhibition of K^+ secretion.

In contrast to the action of TMP on the apical membrane, TMP at 10^{-3} *M* in the bath caused a slight but significant depolarization of V_T and V_B without changes in R_T or fR_A. The findings suggest that TMP may act on the basolateral membrane of the CD cell and inhibit an electrogenic Na^+ transport system, possibly the Na^+-K^+ pump activity. This is supported by the report of Eiam-Ong et al. [11], in which, when CCD segments isolated from normal rat kidneys were incubated with 10^{-4} *M* TMP for 90 min, their Na^+-K^+-ATPase activities decreased by 30%, although the inhibitory effect of TMP at 10^{-4} *M* on Na^+-K^+-ATPase activity in the rat CCD was much greater than that of TMP at 10^{-3} *M* on basolateral Na^+-K^+ pump activity in the rabbit CCD (fig. 7; table 5).

SMX at 10^{-3} *M* in the lumen or bath had no effects on barrier voltages or resistances. Therefore, SMX in the lumen or bath had no effect on CD cell at all. Similarly, no effect of either apical or basolateral addition of SMX on amiloride-sensitive short circuit current [1] or highly selective Na^+ channel activity [10] has been reported in A6 cell monolayers. Furthermore, there was no interaction between TMP and SMX in the lumen (fig. 3; table 2).

The current study demonstrated that TMP at 10^{-3} *M* acts on both apical and basolateral membranes by different mechanisms, however, the question arises as to which action contributes to the TMP-induced hyperkalemia. When 800 mg of SMX is given with 160 mg of TMP twice daily, the peak concentration of TMP in plasma is approximately 6.8×10^{-6} *M* [19]. Peak plasma concentration of TMP is 1.1×10^{-5} *M* after intravenous infusion of 800 mg of SMX and 160 mg of TMP over a period of 1 h [20]. These reports indicate that plasma concentrations of TMP do not reach as high as 10^{-3} *M*. Also, the effects of TMP at 10^{-3} *M* in the bath on V_T and V_B were trivial (fig. 7; table 5). Therefore, the basolateral action is unlikely to contribute to the TMP-induced hyperkalemia. On the other hand, patients receiving 320 mg of oral TMP per day in two doses have mean urinary TMP concentrations of 2×10^{-4} *M* [20]. It has been shown that the urinary concentrations of TMP may reach 1.1×10^{-3} *M* after a single oral dose of 200 mg TMP in humans [8]. In humans, TMP has a half-life of 8 to 12 h and 80% is excreted unchanged into the urine [21]. Therefore, the concentrations of TMP indeed can reach the level of 10^{-5} to 10^{-3} *M* in the lumen of the CCD, exerting natriuresis and antikaliuresis. Eiam-Ong et al. [11] also reported that acute and chronic administration of TMP into rats decreased Na^+-K^+-ATPase activity in the CCD. This inhibitory action of TMP on Na^+-K^+-ATPase in the CCD can be secondary to its direct effect on apical Na^+ conductance, because apical Na^+ entry is known to modulate basolateral Na^+-K^+ pump activity in the CCD [14, 22].

In conclusion, TMP mainly acts on the apical membrane of the rabbit CD cell, and inhibits macroscopic Na^+ conductance. This effect causes a decrease in the net driving force for K^+ exit across the apical membrane, leading to an inhibition of K^+ secretion.

Acknowledgments

This work was supported in part by Grants-in-Aid from the Ministry of Education, Science, Culture, Sports, Science, and Technology of Japan.

References

1 Choi MJ, Fernandez PC, Patnaik A, Coupaye-Gerard B, D'Andrea D, Szerlip H, Kleyman TR: Brief report: trimethoprim-induced hyperkalemia in a patient with AIDS. N Engl J Med 1993;328:703–706.
2 Greenberg S, Reiser IW, Chou SY: Hyperkalemia with high dose trimethoprim-sulfamethoxazole. Am J Kid Dis 1993;22:603–606.
3 Greenberg S, Reiser IW, Chou SY, Porush JG: Trimethoprim-sulfamethoxazole induces reversible hyperkalemia. Ann Intern Med 1996; 124:316–320.
4 Alappan R, Perazella MA, Buller GK: Hyperkalemia in hospitalized patients treated with trimethoprim-sulfamethoxazole. Ann Intern Med 1996;124:316–320.
5 Kalin MF, Poretsky L, Seres DS, Zumoff B: Hyporeninemic hypoaldosteronisms associated with acquired immune deficiency syndrome. Am J Med 1987;82:1035–1038.
6 Grinspoon SK, Bilezikian JP: HIV disease and endocrine system. N Engl J Med 1992;327: 1360–1365.
7 Fonseca PD, Moura TF, Ferreira KTG: The effect of trimethoprim on sodium transport across the frog skin epithelium. Eur J Pharmacol 1991;207:337–343.
8 Velázquez H, Perazella MA, Wright FS, Ellison DH: Renal mechanism of trimethoprim-induced hyperkalemia. Ann Intern Med 1993; 119:296–301.
9 Muto S: Potassium transport in the mammalian collecting duct. Physiol Rev 2001;81:85–116.
10 Schlanger LE, Kleyman TR, Ling BN: K^+-sparing diuretics actions of trimethoprim: Inhibition of Na^+ channels in A6 distal nephron cells. Kidney Int 1994;45:1070–1076.
11 Eiam-Ong S, Kurtzman NA, Sabatini S: Studies on the mechanisms of trimethoprim-induced hyperkalemia. Kidney Int 1996;49: 1372–1378.
12 Muto S, Yasoshima K, Yoshitomi K, Imai M, Asano Y: Electrophysiological identification of α- and β-intercalated cells and their distribution along the rabbit distal nephron segments. J Clin Invest 1990;86:1829–1839.
13 Muto S, Miyata Y, Asano Y: Electrical properties of the rabbit cortical collecting duct from obstructed and contralateral kidneys after unilateral ureteral obstruction. J Clin Invest 1993; 92:571–581.
14 Muto S, Asano Y, Seldin D, Giebisch G: Basolateral Na^+ pump modulates apical Na^+ and K^+ conductances in rabbit cortical collecting ducts. Am J Physiol 1999;276:F143–F158.
15 Muto S, Asano Y, Wang WH, Seldin D, Giebisch G: Activity of the basolateral K^+ channel is coupled to the Na^+-K^+-ATPase in the cortical collecting duct. Am J Physiol 2003; 285:F945–F954.
16 Tsuruoka S, Muto S, Taniguchi J, Suzuki M, Imai M: Effects of glucocorticoid and mineralocorticoid on potassium transport in the rat medullary thick ascending limb of Henle's loop. Kidney Int 1995;47:802–810.
17 Matsumoto N, Tsuruoka S, Iwamoto T, Tomich JM, Ito K, Imai M, Suzuki M: Expression of an artificial Cl^- channel in microperfused renal proximal tubules. J Membr Biol 2003;193:195–200.
18 Giebisch G: A trail of research on potassium. Kidney Int 2002;62:1498–1512.
19 Petri WA Jr: Antimicrobial agents: sulfonamide, trimethoprim-sulamethoxazole, quinolone, and agents for urinary tract infections: trimethoprim-sulfamethoxazole; in Hardman JG, Limbird LE (eds): Goodman & Gilman's The Pharmacological Basis of Therapeutics, ed 10. New York, MacGraw-Hill, 2001, pp 1176–1179.
20 Berns JS, Cohen RM, Stumacher RJ, Rudnick MR: Renal aspects of therapy for human immunodeficiency virus and associated opportunistic infections. J Am Soc Nephrol 1991;1: 1061–1080.
21 Sharpstone P: The renal handling of trimethoprim and sulfamethoxazole in man. Postgrad Med J 1969;45:S38–S42.
22 Horisberger JD, Giebisch G: Intracellular Na^+ and K^+ activities and membrane conductances in the collecting tubule of amphiuma. J Gen Physiol 1988;92:643–665.

Eur J Clin Pharmacol (2006) 62: 209–215
DOI 10.1007/s00228-005-0071-1

PHARMACOKINETICS AND DISPOSITION

Koh-ichi Sugimoto · Nobutaka Araki · Masami Ohmori · Ken-ichi Harada · Yimin Cui · Shuichi Tsuruoka · Atsuhiro Kawaguchi · Akio Fujimura

Interaction between grapefruit juice and hypnotic drugs: comparison of triazolam and quazepam

Received: 17 October 2005 / Accepted: 14 November 2005 / Published online: 17 January 2006

Abstract *Objective:* Grapefruit juice (GFJ) inhibits cytochrome P450 (CYP) 3A4 in the gut wall and increases blood concentrations of CYP3A4 substrates by the enhancement of oral bioavailability. The effects of GFJ on two benzodiazepine hypnotics, triazolam (metabolized by CYP3A4) and quazepam (metabolized by CYP3A4 and CYP2C9), were determined in this study. *Methods:* Nine healthy subjects were administered 0.25 mg triazolam or 15 mg quazepam, with or without GFJ. Each trial was performed using an open, randomized, cross-over design with an interval of more than 2 weeks between trials. Blood samples were obtained during the 24-h period immediately following the administration of each dose. Pharmacodynamic effects were determined by the digit symbol substitution test (DSST) and utilizing a visual analog scale. *Results:* GFJ increased the plasma concentrations of both triazolam and quazepam and of the active metabolite of quazepam, 2-oxoquazepam. The area under the curve (AUC)(0–24) of triazolam significantly increased by 96% ($p<0.05$). The AUC(0–24) of quazepam (+38%) and 2-oxoquazepam (+28%) also increased; however, these increases were not significantly different from those of triazolam. GFJ deteriorated the performance of the subjects in the DSST after the triazolam dose (−11 digits at 2 h after the dose, $p<0.05$), but not after the quazepam dose. Triazolam and quazepam produced similar sedative-like effects, none of which were enhanced by GFJ. *Conclusion:* These results suggest that the effects of GFJ on the pharmacodynamics of triazolam are greater than those on quazepam. These GFJ-related different effects are partly explained by the fact that triazolam is presystemically metabolized by CYP3A4, while quazepam is presystemically metabolized by CYP3A4 and CYP2C9.

Keywords Grapefruit juice · CYP3A4 · CYP2C9 · Triazolam · Quazepam

K.-i. Sugimoto · N. Araki · M. Ohmori · K.-i. Harada · Y. Cui · S. Tsuruoka · A. Kawaguchi · A. Fujimura (✉)
Division of Clinical Pharmacology,
Department of Pharmacology,
Jichi Medical School,
3311-1 Minamikawachi,
Tochigi, 329-0498, Japan
e-mail: akiofuji@jichi.ac.jp
Tel.: +81-285-587387
Fax: +81-285-44-7562

Introduction

The ingestion of grapefruit juice (GFJ) increases the oral bioavailability of a number of drugs, including felodipine, terfenadine, cyclosporine and simvastatin [1–4]. The mechanism by which GFJ substantially reduces the oral clearance of these cytochrome P450 (CYP) 3A4 substrate drugs is by increasing their oral bioavailability through a post-transcriptional mechanism that decreases CYP3A4 protein content in the small intestine [5]; hepatic CYP3A4 activity is not blunted by GFJ [5]. Furanocoumarin-induced inhibition of CYP3A4 is thought to be involved in the drug-food interaction [6, 7].

Triazolam and quazepam are benzodiazepine derivatives which are frequently prescribed for the treatment of sleep disorders. In an in vitro study, von Moltke et al. demonstrated that triazolam is metabolized by CYP3A4 to α-hydroxytriazolam and 4-hydroxytriazolam [8]. As expected, GFJ has been found to increase plasma triazolam concentration and enhance its pharmacodynamic effects in human subjects [9, 10]. However, because the metabolism of quazepam to 2-oxoquazepam is mediated by CYP3A4 and CYP2C9 [11], it is anticipated that the effects of GFJ on the pharmacokinetics and pharmacodynamics of triazolam may be greater than those on quazepam. This study was undertaken to examine this hypothesis. The effects of GFJ on the pharmacokinetics and pharmacodynamics of triazolam and quazepam were determined by an open, randomized, cross-over design in healthy subjects.

Methods

Study design

The study was performed in an open, randomized, crossover design with four phases. The interval between each phase (study day) was more than 2 weeks. The protocol was approved by the Ethics Committee of Jichi Medical School (Tochigi, Japan).

Nine healthy Japanese men (age: 23–44 years old; weight: 56–80 kg) participated in this study after giving written informed consent. Genetic analysis [12] showed that all subjects were extensive metabolizers of CYP2C9 substrates. Four of the participants were smokers. The subjects were instructed not to take any medications, herbal dietary supplements and herbal tea throughout the study period. The consumption of GFJ was not allowed during the entire study period, except for when a trial was being conducted, while the consumption of caffeine-containing beverages, including coffee and green tea, and alcohol and smoking were prohibited from one night before the trial until a final blood sampling on the next morning. The subjects were given 250 ml of normal-strength GFJ (Tropicana, Kirin Beverage, Tokyo, Japan) three times daily for 3 days immediately prior to the trial according to a randomized schedule. The recommended dose for the treatment of sleep disorders in Japan is 0.25–0.5 mg triazolam and 15–30 mg quazepam. However, because 0.25 mg triazolam and 15 mg quazepam are most frequently used as initial doses, we chose these doses for the trials. On the day of the trial, subjects took a single oral dose of triazolam (0.25 mg; Halcion, Pharmacia & Upjohn, Tokyo, Japan) or quazepam (15 mg; Doral; Mitubishi Pharma, Tokyo, Japan) together with 250 ml of GFJ or water at 8:00 A.M. after an overnight fast. In the trials with GFJ, the subjects also took 250 ml of GFJ 4 and 12 h after the drug had been taken. The subjects had a light meal 4 h after taking either the triazolam or quazepam.

Blood sampling

Blood samples (5 ml in each) for the analyses of triazolam and quazepam were collected in heparinized tubes immediately before and at 0.5, 1, 2, 3, 4, 6, 8, 12 and 24 h after the participants had taken the doses of triazolam or quazepam. Plasma samples were stored at −80°C until the assay was carried out.

Pharmacodynamic measurements

The pharmacodynamic effects of triazolam and quazepam were determined using the digit symbol substitution test (DSST) [13] and a visual analog scale (VAS) immediately before each blood sampling and from 0–12 h following the administration of the drug. In the DSST, the participants in the study substituted simple digit symbols using a pencil and paper. The number of digits correctly substituted in 2 min was recorded. Subjective assessments were made on 100-mm long horizontal ungraded visual analogue scales. Sedative-like effects observed were the pairs of adjectives (in Japanese) such as drowsy/alert, calm/nervous, clumsy/skilled, mentally slow/quick-witted and discontented/contented. The subjects had been trained to perform the tests before the initiation of the study: prior to the trials they performed DSST several times after being given oral instructions; thereafter, they completed 12 h of baseline study (DSST and VAS) without medication on a different day.

Assay of plasma triazolam

Plasma concentration of triazolam was measured by a high-performance liquid chromatography (HPLC) method developed in our laboratory. A 2-ml plasma sample was added to 4 ml of methanol, and the mixture was then shaken vigorously for 10 min, followed by centrifugation at 1,500 *g* for 10 min. The procedure was repeated three times, and the supernatant was evaporated to dryness under nitrogen stream. The residue was reconstituted with 100 μl ethanol, and the whole amount was subjected by analysis using a two-step drug extraction process by HPLC.

The HPLC system consisting of a chromatography pump (PU-880; Jasco, Tokyo, Japan), an ultraviolet detector (Uvidec 875; Jasco) and a column (Fine Pak SilC18T5, 5 μm, 250×4.6 mm; Jasco) was used to separate triazolam. The column temperature was set at 40°C with a column oven module. In the first process, the mobile phase consisted of methanol/H_2O (70:30, v/v). The fraction containing triazolam was separated from the interfering substances existing in the residue by collecting the effluent between 6.0 and 7.5 min after the injection. The collected effluent was evaporated to dryness and reconstituted with 100 μl of a mobile phase consisting of methanol/H_2O (54.5:45.5, v/v), which was then injected into the identical HPLC system with the mobile phase. To reduce sample loss, the tube containing the residue obtained in the first process was again washed with the mobile phase, and this reconstituent (100 μl) was also applied to the second separation process. Triazolam was separated out by collecting effluent between 12.0 and 13.5 min. The mobile phase was pumped at a flow rate of 1.0 ml/min for the separation of triazolam. The absorbance of the effluent was monitored at 220 nm.

The effluent containing triazolam was evaporated to dryness and reconstituted with 50 μl of internal standard (1 μg/ml butyl *p*-hydroxybenzoate in methanol), and 20-μl aliquots were applied to the HPLC system. The HPLC system was identical to that described above except for the mobile phase [methanol/H_2O (52.4:47.6, v/v)]. The recovery of 2.5 ng/ml triazolam was 88.7% (n=6). The method was validated for the concentration range from 0.5 to 2.5 ng/ml. The intra-assay coefficient and accuracy were less than 8.6% and 85.1–108.4% (n=6), respectively. The inter-assay coefficient and accuracy were less than 18.8% and 73.4–137.4% (n=6), respectively. The lower detection limit was 0.15 ng/ml.

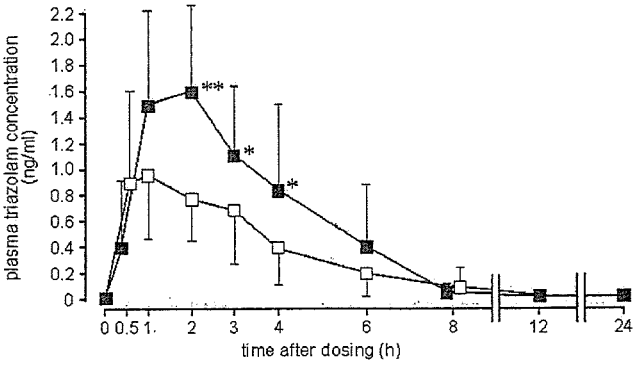

Fig. 1 Plasma concentrations of triazolam after a single oral dose of 0.25 mg triazolamwith grapefruit juice (*black squares*) or water (*open squares*). Points represent the mean (n=9) ± SD. *p<0.05, **p<0.01 versus the control (water) values

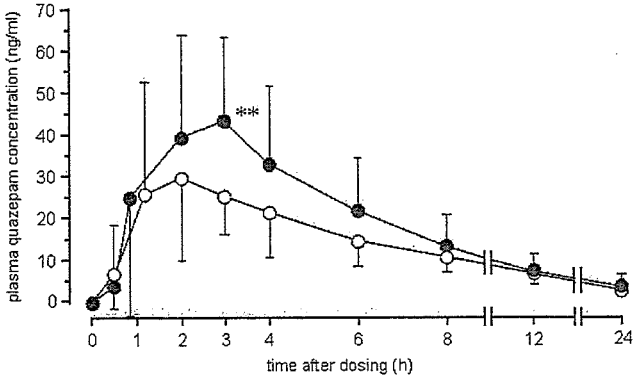

Fig. 2 Plasma concentrations of quazepam after a single oral dose of 15 mg quazepam with grapefruit juice (*black circles*) or water (*open circles*). Points represent the mean (n=9) ± SD. **p<0.01 versus the control (water) values

Assay of plasma quazepam and its metabolites, 2-oxoquazepam and *N*-desmethyl-2-oxoquazepam

Plasma concentrations of quazepam and its metabolites were measured by a column-switching HPLC analysis. An aliquot of each plasma sample (1.5 ml), to which 0.1 ml of cisapride (800 ng/ml) was added as an internal standard, was first alkalinized by adding 500 µl 0.5 *M* NaOH followed by the addition of 0.4 ml H_20 and 5 ml of toluene/chloroform (85:15, v/v). The mixture was shaken vigorously for 15 min and then centrifuged at 2,000 *g* for 10 min. A 4.5-ml portion of the organic layer was evaporated to dryness in vacuo at 45°C. The residue was reconstituted with 0.8 ml of eluent A (see below) and used as an extract.

A 0.5-ml aliquot of the extract was injected onto the column-switching HPLC system which consisted of a chromatography pump (LC-10A; Shimadzu, Tokyo, Japan), an autoinjector (AS-8020; Tosoh, Tokyo, Japan) and an ultraviolet detector (SPD-10A; Shimadzu). Column I (TSK-BSA-C8, 5 µm, 10×4.6 mm; Tosoh) was used for pretreatment and column II (STR-ODS II, 5 µm, 150×4.6 mm; Shimadzu) for the separation of quazepam and 2-oxoquazepam. The column temperature was set at 30°C with a column oven module. Between 0 and 13.0 min after the injection of a sample, cisapride was separated from the interfering substances present in the extract on column I by means of a mobile phase solvent (eluent A) consisting of acetnitrile/0.02 mol/l KH_2PO_4 (13:87, v/v). Between 13.0 and 20.0 min after the injection, quazepam and its metabolites, which had been retained on column I were eluted with a mobile phase (eluent B) consisting of acetnitrile/perchloric acid/0.02 mol/l KH_2PO_4 (41.00:0.05:58.95, v/v/v), and the effluent from column I was switched to column II. Then *N*-desmethyl-2-oxoquazepam was separated on column II by eluting with eluent B (between 20.0 and 32.0 min). Quazepam and 2-oxoquazepam were separated on column II by eluting with a mobile phase solvent (eluent C) consisting of acetnitrile/0.02 mol/l KH_2PO_4 (62.5:37.5, v/v) between 32.0 and 46.5 min. The mobile phase was pumped at a flow rate of 0.6 ml/min. The absorbance of the effluent from column II was monitored at 254 nm for the metabolites and 286 nm for quazepam.

The lower detection limits were 0.8 ng/ml, with a linear calibration range from 1 to 100 ng/ml of quazepam and its metabolites. The recoveries of quazepam and its metabolites was more than 93.2% at 10 ng/ml of the concentrations (n=6). The inter-and intra-assay coefficient of variations were less than 4.6% at 10 ng/ml of these compounds.

Pharmacokinetic calculations

Pharmacokinetics were characterized by maximum plasma concentration C_{max}), time to maximum plasma concentra-

Table 1 Pharmacokinetic parameters[a] of triazolam, quazepam and 2-oxoquazepam after a single oral dose of the drug (0.25 mg triazolam or 15 mg quazepam) with grapefruit juice (GFJ) or water in nine healthy Japanese male volunteers

	C_{max} (ng/ml)			t_{max} (h)		AUC(0–24) (ng h/ml)		
	Water	GFJ	Ratio	Water	GFJ	Water	GFJ	Ratio
Triazolam	1.3±0.4[b]	1.9±0.6*	1.55±0.46 (1.27; 1.84)	1.4±1.0	1.6±0.5	6.3±2.7	10.9±4.0*	1.96±1.02 (1.34; 2.59)
Quazepam	36.9±21.7	52.0±20.8*	1.62±0.59 (1.25; 2.00)	2.2±1.0	2.6±0.7	247.5±110.2	324.2±150.1	1.38±0.43 (1.12; 1.64)
2-Oxoquazepam	6.1±1.4	9.7±3.5*	1.57±0.36 (1.35; 1.79)	2.4±1.0	2.4±0.9	53.5±14.8	67.6±24.5	1.28±0.34 (1.07; 1.50)

*p<0.05 versus water

[a] C_{max}, Maximum plasma concentration; t_{max}, time to maximum concentration; AUC(0–24), area under the plasma concentration time curve from 0 to 24 h after administration of the dose

[b] Values are the mean ± SD (90% confidence interval)

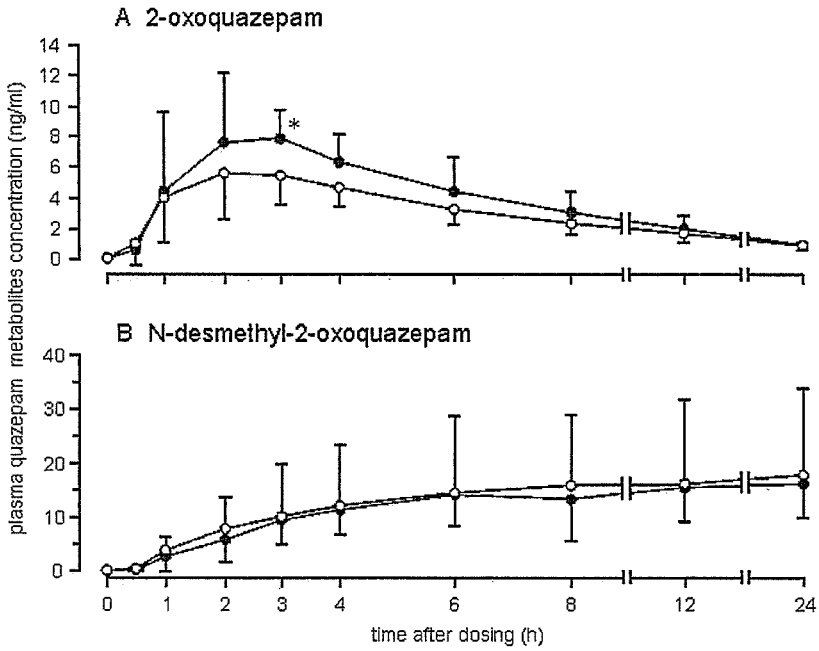

Fig. 3 Plasma concentrations of quazepam metabolites, 2-oxo-quazepam (**a**) and *N*-desmethyl-2-oxoquazepam (**b**), after a single oral dose of 15 mg quazepam with grapefruit juice (*black circles*) or water (*open circles*). Points represent the mean (n=9) ± SD. *p<0.05 versus the control (water) values

tion (t_{max}), elimination half-life ($t_{½}$) and area under the plasma concentration-time curve from 0–24 h post-administration of the drug [AUC(0–24)]. The elimination rate constant (K_e) was determined using last three points of a linear regression analysis of a log-linear phase of the plasma drug concentration-time curve. Elimination half-life ($t_{½}$) was calculated as follows:

$$t_{1/2} = \ln 2/K_e$$

The AUC(0–24) was calculated by the trapezoidal rule.

Statistical analysis

Data are expressed as the mean ± standard deviation (SD). Data were analyzed by paired Student's *t*-test or analysis of variance (ANOVA) using the statistical program *Statview* for Windows, version 5.0 (SAS Institute, Cary, N.C.). A correlation between plasma drug concentrations and the decrease in the number of digit substitutions was analyzed by the Pearson's correlation coefficient. Differences were regarded as statistically significant when the p value was less than 0.05.

Results

Plasma concentration of triazolam

The plasma concentration of triazolam increased after the 0.25 dose had been given with GFJ relative to the same dose given with water (Fig. 1). The C_{max} and AUC(0–24) of the agent were significantly greater with GFJ than with water (Table 1). No significant difference was observed in the $t_{½}$ (in hours) between the two groups (water: 3.6, GFJ: 3.4).

Plasma concentrations of quazepam and 2-oxoquazepam

Plasma concentrations of quazepam and 2-oxoquazepam increased after a dose of quazepam was given with GFJ (Figs. 2 and 3a). The values of C_{max} of these agents in the trial with GFJ were significantly greater than those in the trial with water (Table 1). Their AUC(0–24) were also greater in the trial with GFJ (Table 1), but they did not

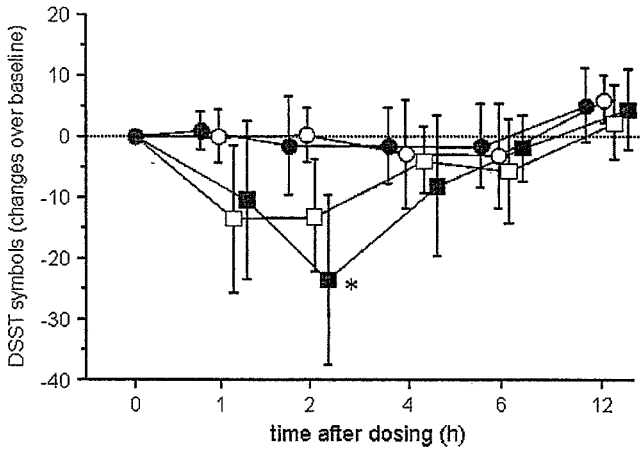

Fig. 4 Digit symbol substitution test (DSST, expressed as changes over the predose baseline) after a single oral dose of 0.25 mg triazolam or 15 mg quazepam with grapefruit juice or water. *Open circle* Quazepam with water, *black circle* quazepam with grapefruit juice, *open square* triazolam with water, *closed square* triazolam with grapefruit juice. Points represent the mean (n=9) ± SD. *p<0.05 versus the control (water) values